

Oxidized phospholipids are proinflammatory and proatherogenic in hypercholesterolaemic mice

Xuchu Que¹, Ming-Yow Hung^{1,9,10}, Calvin Yeang¹, Ayelet Gonen¹, Thomas A. Prohaska¹, Xiaoli Sun¹, Cody Diehl^{1,11}, Antti Määttä², Dalia E. Gaddis³, Karen Bowden¹, Jennifer Pattison¹, Jeffrey G. MacDonald⁴, Seppo Ylä-Herttuala², Pamela L. Mellon⁵, Catherine C. Hedrick³, Klaus Ley³, Yury I. Miller¹, Christopher K. Glass^{1,6}, Kirk L. Peterson¹, Christoph J. Binder^{7,8}, Sotirios Tsimikas¹ & Joseph L. Witztum^{1*}

Oxidized phospholipids (OxPL) are ubiquitous, are formed in many inflammatory tissues, including atherosclerotic lesions, and frequently mediate proinflammatory changes¹. Because OxPL are mostly the products of non-enzymatic lipid peroxidation, mechanisms to specifically neutralize them are unavailable and their roles in vivo are largely unknown. We previously cloned the IgM natural antibody E06, which binds to the phosphocholine headgroup of OxPL, and blocks the uptake of oxidized low-density lipoprotein (OxLDL) by macrophages and inhibits the proinflammatory properties of OxPL^{2–4}. Here, to determine the role of OxPL in vivo in the context of atherogenesis, we generated transgenic mice in the *Ldlr*^{-/-} background that expressed a single-chain variable fragment of E06 (E06-scFv) using the *ApoE* promoter. E06-scFv was secreted into the plasma from the liver and macrophages, and achieved sufficient plasma levels to inhibit in vivo macrophage uptake of OxLDL and to prevent OxPL-induced inflammatory signalling. Compared to *Ldlr*^{-/-} mice, *Ldlr*^{-/-}E06-scFv mice had 57–28% less atherosclerosis after 4, 7 and even 12 months of 1% high-cholesterol diet. Echocardiographic and histologic evaluation of the aortic valves demonstrated that E06-scFv ameliorated the development of aortic valve gradients and decreased aortic valve calcification. Both cholesterol accumulation and in vivo uptake of OxLDL were decreased in peritoneal macrophages, and both peritoneal and aortic macrophages had a decreased inflammatory phenotype. Serum amyloid A was decreased by 32%, indicating decreased systemic inflammation, and hepatic steatosis and inflammation were also decreased. Finally, the E06-scFv prolonged life as measured over 15 months. Because the E06-scFv lacks the functional effects of an intact antibody other than the ability to bind OxPL and inhibit OxLDL uptake in macrophages, these data support a major proatherogenic role of OxLDL and demonstrate that OxPL are proinflammatory and proatherogenic, which E06 counteracts in vivo. These studies suggest that therapies inactivating OxPL may be beneficial for reducing generalized inflammation, including the progression of atherosclerosis, aortic stenosis and hepatic steatosis.

Oxidation of LDL, a central event in atherogenesis, results in formation of neo-epitopes from lipid peroxidation, termed ‘oxidation-specific epitopes’, which are endogenous ‘danger-associated molecular patterns’ recognized by multiple innate pattern recognition receptors^{1,5}. Phosphocholine-containing OxPL are a notable example, and the phosphocholine headgroup of OxPL in OxLDL (as a lipid or OxPL–protein adduct) is recognized by macrophage scavenger receptors and Toll-like receptors (TLRs), by the innate protein CRP and by the IgM natural antibody E06¹. OxPL accumulate in OxLDL, apoptotic cells and microparticles that are released by activated and dying cells^{4,6} and are

ubiquitous in a wide variety of inflammatory settings, including atherosclerosis⁷, pulmonary^{8,9} and neurological diseases^{10–12} and non-alcoholic steatohepatitis (NASH)¹³ among others¹. In addition, OxPL present on lipoprotein(a) are thought to mediate, in part, the ability of lipoprotein(a) to promote atherogenesis and calcific aortic valve disease¹⁴. However, the pathophysiological effects of endogenously generated OxPL in vivo are unknown and it is unlikely that they could be specifically neutralized in vivo by small molecules or enzyme inhibitors.

The natural antibody E06 recognizes the hydrophilic phosphocholine headgroup of OxPL that are present in OxLDL and apoptotic cells but does not recognize unoxidized PL in LDL or viable cells. Furthermore, E06 blocks uptake of OxLDL by macrophages in vitro and can inhibit many proinflammatory properties of OxPL (a detailed characterization of E06 can be found in the Supplementary Information). To determine the role of OxPL in vivo in atherogenesis, we generated transgenic mice expressing a single chain variable fragment of E06 (E06-scFv) as described in the Methods (Extended Data Fig. 1a–c). The E06-scFv cDNA was inserted into a liver-specific expression vector, pLiv7, under the *ApoE* promoter and a hepatic control element enhancer (LE6) (Fig. 1a) and used to generate E06-scFv transgenic mice in the C57BL/6 background. These were crossbred to generate ‘homozygous’ mice, which were bred with *Ldlr*^{-/-} and *Rag1*^{-/-}*Ldlr*^{-/-} mice on the C57BL/6 background. The E06-scFv mRNA showed the highest expression in the liver, macrophages and spleen, and low-level expression was found in the heart, lung, kidney and brain (Extended Data Fig. 1d). The plasma E06-scFv levels in the various transgenic models studied were 20–30 µg ml⁻¹. Plasma titres of endogenous IgM E06 were not affected by the E06-scFv transgene in the various studies described (Extended Data Fig. 2). Binding and competition studies validated that plasma E06-scFv fully replicated the binding properties of the parent E06 IgM, specifically binding to various phosphocholine epitopes as well as OxLDL and a POVPC peptide, (a synthetic oxPL–peptide analogue¹⁵) and to AB1-2, a highly specific T15/E06 anti-idiotypic antibody (Fig. 1b and Extended Data Fig. 1e). Even at high dilutions (1:100), plasma from *Ldlr*^{-/-}E06-scFv mice inhibited binding of biotinylated OxLDL to J774 macrophages in culture by more than 75% (Fig. 1c). E06-scFv also inhibited the proinflammatory activation of thioglycollate-elicited macrophages (TGEM) when oxidized PAPC (oxPAPC) was injected in vivo. Expression of both TNFα and IL-1β was markedly attenuated in TGEM from *Ldlr*^{-/-}E06-scFv mice (Fig. 1d). E06-scFv-enriched plasma bound to rabbit atherosclerotic tissue (Extended Data Fig. 3a), and also prominently stained late stage apoptotic cells but not viable cells (Extended Data Fig. 3b, c). Phosphocholine-keyhole limpet haemocyanin (KLH) effectively abolished E06-scFv binding in both cases (data not shown). We also demonstrated the presence of E06-scFv antibody in aortic roots

¹Department of Medicine, University of California, San Diego, La Jolla, CA, USA. ²A.I. Virtanen Institute, University of Eastern Finland, Kuopio, Finland. ³La Jolla Institute for Allergy and Immunology, La Jolla, CA, USA. ⁴Center for Human Nutrition, UT Southwestern Medical Center, Dallas, TX, USA. ⁵Department of Reproductive Medicine, University of California, San Diego, La Jolla, CA, USA. ⁶Department of Cellular and Molecular Medicine, University of California, San Diego, La Jolla, CA, USA. ⁷Department of Laboratory Medicine, Medical University of Vienna, Vienna, Austria. ⁸Center for Molecular Medicine of the Austrian Academy of Sciences, Vienna, Austria. ⁹Present address: Department of Internal Medicine, School of Medicine, College of Medicine, Taipei Medical University, Taipei City, Taiwan. ¹⁰Present address: Division of Cardiology, Department of Internal Medicine, Shuang Ho Hospital, Taipei Medical University, New Taipei City, Taiwan. ¹¹Present address: Brigham Young University Idaho, Rexburg, ID, USA. *e-mail: jwitztum@ucsd.edu

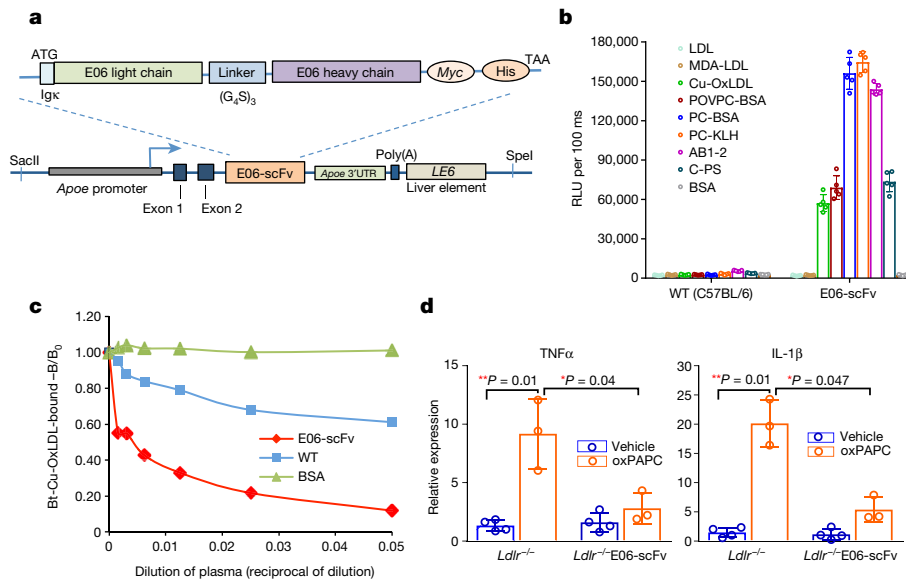


Fig. 1 | Transgenic mice expressing a single-chain variant of E06 (E06-scFv). **a**, The configuration of the E06 single-chain transgene, which encodes the E06 light and heavy chains with a flexible 15-amino acid linker (Gly₄Ser)₃ and epitope tags under the direction of the *Apoe* promoter and LE6 enhancer. UTR, untranslated region. **b**, Binding properties of plasma from wild-type (WT) C57BL/6 and E06-scFv-expressing mice to indicated antigens. RLU, relative light units. Data are mean \pm s.e.m., $n = 5$ plasma samples from each group, each point was determined in triplicate. **c**, Plasma from E06-scFv-expressing mice reduced OxLDL binding by macrophages in culture. Bt-Cu-OxLDL, biotinylated OxLDL. One experiment representative of five separate experiments is shown and each point was determined in triplicate.

of *Ldlr*^{-/-}E06-scFv mice, consistent with either a plasma origin or local macrophage secretion (Extended Data Fig. 3d).

To determine the effect of OxPL on atherosclerosis, *Ldlr*^{-/-} and *Ldlr*^{-/-}E06-scFv mice were fed a high-cholesterol diet (HCD) for 4, 7 or 12 months. Weight gain, plasma cholesterol, triglycerides and lipoprotein profiles were similar (Extended Data Table 1 and Extended Data Fig. 4). Compared to *Ldlr*^{-/-} mice, atherosclerosis was significantly reduced in *Ldlr*^{-/-}E06-scFv mice at each time point (per cent of aortic surface involved by en face analysis was reduced by 57%, 34% and 28%, and aortic root by 55%, 41% and 27%, respectively, at 4, 7 and 12 months; Fig. 2c, d). OxPL have been shown to promote apoptosis and necrosis^{1,16}. In lesion size-matched cross-sections, necrotic core areas were 44% smaller ($P = 0.015$) and had visibly more collagen in *Ldlr*^{-/-}E06-scFv mice, suggesting improved plaque stability (Extended Data Fig. 5a).

The *Apoe* promoter is known to be active in macrophages and to respond to cholesterol and LXR agonists¹⁷. Peritoneal macrophages from *Ldlr*^{-/-}E06-scFv mice expressed E06-scFv mRNA, and enzyme-linked immunosorbent assay (ELISA) analysis of culture supernatants demonstrated the binding of secreted E06-scFv to phosphocholine-bovine serum albumin (BSA) (Extended Data Fig. 5b). The LXR agonist T0901317 enhanced synthesis and secretion of bioactive E06-scFv into the culture medium (Extended Data Fig. 5b), demonstrating a functional *Apoe* promoter regulating expression of the E06-scFv in macrophages. To determine the contribution of macrophage E06-scFv to atheroprotection, we performed a bone marrow transplantation (BMT) from C57BL/6 wild-type or from E06-scFv mice (not on *Ldlr*^{-/-} background) into irradiated male *Ldlr*^{-/-} recipients and fed the mice with a Western diet. Plasma E06-scFv titres were detectable in recipient *Ldlr*^{-/-} mice two weeks after BMT and rose in response to cholesterol feeding (Extended Data Fig. 5c), but even at 16 weeks were only around 10% of those observed in the *Ldlr*^{-/-}E06-scFv mice. Nevertheless, aortic root lesions were reduced by 37% in mice receiving bone marrow from E06-scFv donors, compared to wild-type donors

(Extended Data Fig. 5d). Plasma lipids were not different (Extended Data Table 1). These data suggest an important role for local arterial macrophage secretion of E06-scFv in providing atheroprotection, although conceivably some of the benefits of E06-scFv could derive from macrophages engrafted in other tissues.

To provide insights into atheroprotective mechanisms, we demonstrated decreased *in vivo* macrophage uptake of fluorescently labelled OxLDL in *Ldlr*^{-/-}E06-scFv mice. We used *Rag1*^{-/-}*Ldlr*^{-/-} mice to exclude effects of other antibodies and allow an examination of the protective effect of the E06-scFv alone. Uptake of OxLDL was significantly reduced in macrophages of *Rag1*^{-/-}*Ldlr*^{-/-}E06-scFv mice compared to *Rag1*^{-/-}*Ldlr*^{-/-} mice (Fig. 3a). To assess the full potential of E06-scFv to bind to OxLDL, we pre-incubated plasma from *Ldlr*^{-/-}, *Rag1*^{-/-}*Ldlr*^{-/-} or *Rag1*^{-/-}*Ldlr*^{-/-}E06-scFv mice with the OxLDL before injection. Whereas macrophage uptake of OxLDL was approximately 100% or around 70% for OxLDL incubated with *Rag1*^{-/-} or *Rag1*^{-/-}*Ldlr*^{-/-} plasma, respectively, it was reduced to around 26% when pre-mixed with *Rag1*^{-/-}*Ldlr*^{-/-}E06-scFv plasma (Fig. 3b). Consistent with the decreased *in vivo* uptake of OxLDL, macrophage cholesterol content of *Ldlr*^{-/-}E06-scFv mice was reduced by 48% compared to *Ldlr*^{-/-} mice ($P = 0.02$; Fig. 3c). Desmosterol was reported to be increased in macrophages from Western diet-fed *Ldlr*^{-/-} mice, leading to decreased inflammatory gene expression¹⁸. However, neither desmosterol nor other oxysterol concentrations were different between macrophages of *Ldlr*^{-/-} and *Ldlr*^{-/-}E06-scFv mice (Extended Data Fig. 1f).

RNA-sequencing analysis of TGEM (Fig. 3d, e) suggested a shift from a more inflammatory 'M1-like' phenotype in the *Ldlr*^{-/-} mice to a more attenuated 'M2-like' repair phenotype in the *Ldlr*^{-/-}E06-scFv mice. Gene Ontology analyses indicated that nearly all the genes expressed more than 1.5-fold higher in the *Ldlr*^{-/-}E06-scFv macrophages relate to immune regulation and defence, of both innate and adaptive immune systems (Extended Data Table 2). We also used flow cytometry to profile arterial wall cells (Fig. 3f). Compared to macrophages isolated

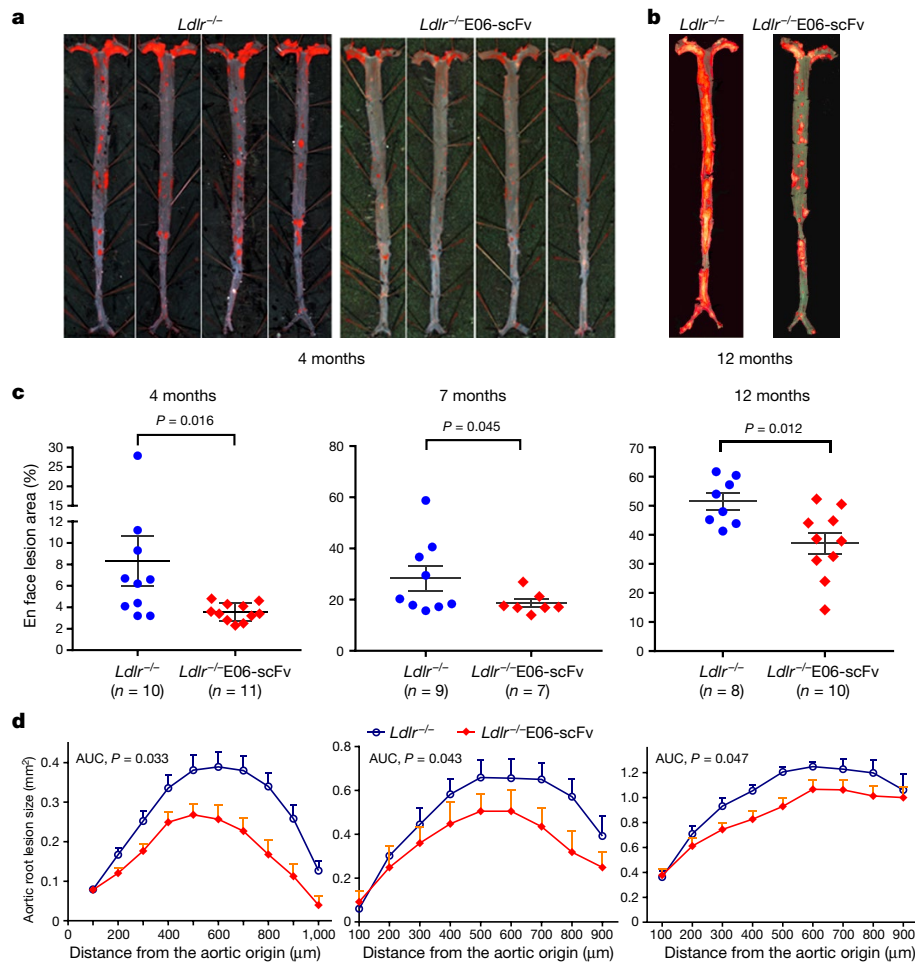


Fig. 2 | E06-scFv reduces atherosclerosis in HCD-fed *Ldlr*^{-/-} mice. **a, **b**, Examples of en face sections showing atherosclerosis in *Ldlr*^{-/-} and *Ldlr*^{-/-}E06-scFv mice after 4 months (**a**) and 12 months (**b**) of 1% HCD. **c**, **d**, Cumulative data for extent of en face lesion formation in the entire aorta (**c**) or at the aortic root (**d**) of *Ldlr*^{-/-} ($n = 8$ –10, as indicated in **c**) and**

Ldlr^{-/-}E06-scFv mice ($n = 7$ –11, as indicated in **c**). Compared to *Ldlr*^{-/-} mice, atherosclerosis was significantly reduced in *Ldlr*^{-/-}E06-scFv mice at 4, 7 and 12 months (en face sections, 57%, 34% and 28%; aortic root, 55%, 41% and 27%, respectively).

from aortas of chow-fed *Ldlr*^{-/-} mice, macrophages from HCD-fed *Ldlr*^{-/-} mice were shifted to a predominant M1-like phenotype (CD45⁺CD11b⁺CD11c⁻Arg1⁻), whereas despite the same cholesterol levels, macrophages from the HCD-fed *Ldlr*^{-/-}E06-scFv mice showed an M2-like phenotype (CD45⁺CD11b⁺CD11c⁻Arg1⁺), more comparable to the profile found in the chow-fed *Ldlr*^{-/-} mice.

Aortas from HCD-fed *Ldlr*^{-/-} mice had greater total monocyte/lymphocyte accumulation than did chow-fed *Ldlr*^{-/-} or HCD-fed *Ldlr*^{-/-}E06-scFv mice, and in particular, a greater enrichment of lymphocytes, especially T but also B cells (Extended Data Table 3). The proportions of CD4⁺ and CD8⁺ T cells in the blood, periaortic lymph nodes and spleens of *Ldlr*^{-/-} and *Ldlr*^{-/-}E06-scFv mice were not different (data not shown). There were no differences between the two groups in red blood cell or white blood cell counts, or in blood coagulation markers including prothrombin time (PT) and activated partial thromboplastin time (aPTT), fibrinogen and plasminogen (data not shown).

Recent genetic data demonstrate a strong causal role for Lp(a) and its associated OxPL in the aetiology of calcific aortic valve disease in humans^{14,19}. We therefore prospectively used M-mode two-dimensional and Doppler ultrasound, to measure gradients at the aortic valves in HCD-fed *Ldlr*^{-/-} and *Ldlr*^{-/-}E06-scFv mice at 6, 9 and 12 months, and at 15 months the calcium content of the aortic valves was evaluated histologically. There was a progressive increase over time in mean aortic valve pressure gradients in *Ldlr*^{-/-} mice, consistent with early restriction of blood flow through the aortic valve, which was significantly

attenuated in the *Ldlr*^{-/-}E06-scFv mice and was 49% lower at 12 months (Fig. 4a, Extended Data Fig. 6a and Extended Data Table 4). Total aortic valve calcium content was also significantly reduced by 41.5% (Fig. 4b, c). Consistent with the more extensive pathology noted in the aortic valve leaflets in the *Ldlr*^{-/-} mice (Fig. 4b and Extended Data Fig. 5a) representative M-mode echocardiography demonstrated thicker aortic valve leaflets in the *Ldlr*^{-/-} mice (Extended Data Fig. 6b). Over 15 months of prospective observation, it was notable that 6 out of 13 *Ldlr*^{-/-} mice died, whereas 0 out of 10 *Ldlr*^{-/-}E06-scFv mice died ($P = 0.016$, Kaplan–Meier survival analysis; Fig. 4d).

Livers of mice on a HCD are known to develop steatosis and accumulate increased levels of oxidation-specific epitopes, including OxPL²⁰. Livers from *Ldlr*^{-/-} mice stained prominently with E06 IgM compared to *Ldlr*^{-/-}E06-scFv livers (Fig. 4f), although hepatocyte-derived E06-scFv may partially mask OxPL epitopes in the livers of *Ldlr*^{-/-}E06-scFv mice. The histological appearance of steatosis in the *Ldlr*^{-/-}E06-scFv livers was decreased, which was confirmed by significant decreases in hepatic triglyceride and cholesterol content (Fig. 4e), and there was decreased inflammatory gene expression in whole-liver extracts (Extended Data Fig. 6c).

Serum amyloid A is known to be raised by cholesterol feeding and reflects a systemic inflammatory status in mice²¹. Notably, despite plasma cholesterol values of more than 800 mg dl⁻¹, plasma serum amyloid A levels were reduced by 32% in *Ldlr*^{-/-}E06-scFv mice ($P = 0.016$) supporting a generalized decrease in systemic inflammation (Fig. 4g).

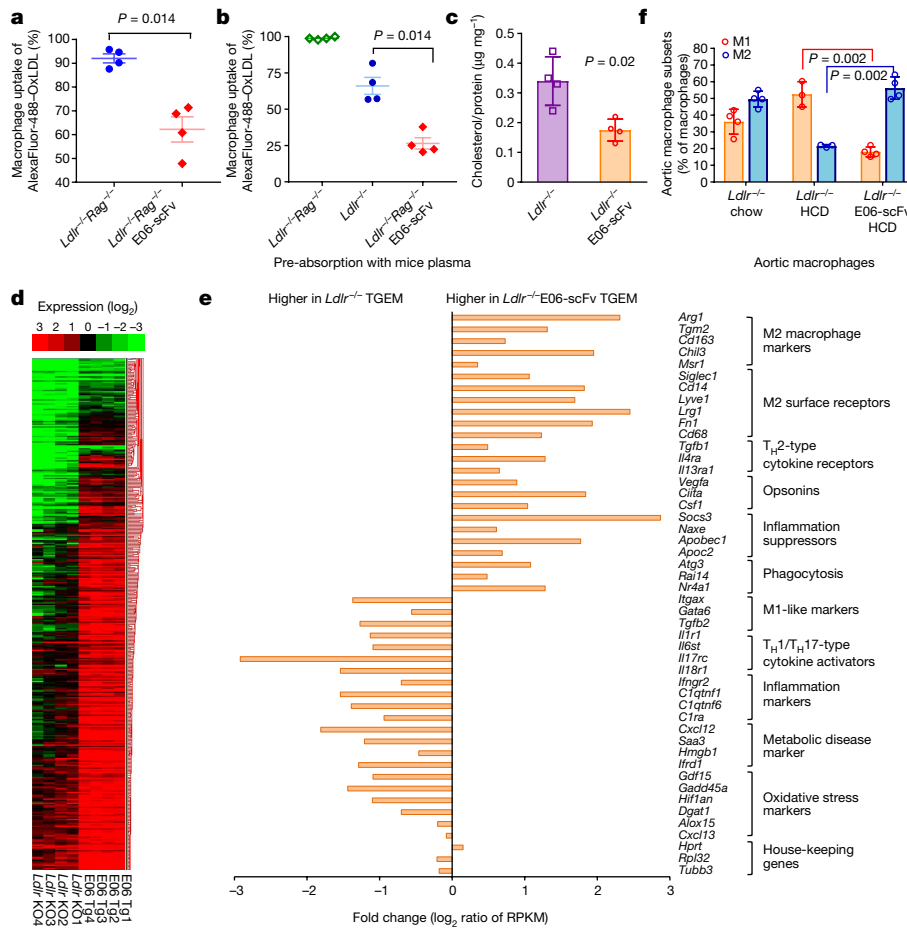


Fig. 3 | Mechanisms by which E06-scFv decreases atherosclerosis.

a, AlexaFluor-488-labelled OxLDL was injected intraperitoneally and macrophage uptake of OxLDL was determined by fluorescence-activated cell sorting (FACS) and expressed as the percentage of macrophages that took up OxLDL. OxLDL uptake by macrophages was reduced in *Ldlr*^{-/-}*Rag1*^{-/-}E06-scFv compared to *Ldlr*^{-/-}*Rag1*^{-/-} mice (percentage uptake, 91 ± 1.03 compared to 62 ± 5.01, *n* = 4 mice per genotype). **b**, AlexaFluor-labelled OxLDL was pre-incubated with plasma from *Ldlr*^{-/-}*Rag1*^{-/-}, *Ldlr*^{-/-} or *Ldlr*^{-/-}*Rag1*^{-/-}E06-scFv mice, and injected into corresponding mice (*n* = 4 per genotype) and uptake by macrophages was determined as in **a**. The percentage of macrophages that took up OxLDL was 98.83 ± 0.44, 66.06 ± 5.87 and 26.48 ± 3.90, respectively. The approximately 25% decrease observed following incubation with *Ldlr*^{-/-} plasma possibly reflects the presence of endogenous anti-OxLDL antibodies. **c**, TGEM from mice fed a HCD for 16 weeks (*n* = 4 mice per genotype) were isolated and cellular levels of cholesterol, desmosterol and

other oxysterols were determined and normalized to cellular protein. Total cholesterol accumulation shown here was reduced by 48% in *Ldlr*^{-/-}E06-scFv mice. Data are mean ± s.d.; *n* = 4. Desmosterol and oxysterol levels were similar (see Extended Data Fig. **d**). **d**, Heat map of RNA-sequencing data from TGEM of *Ldlr*^{-/-} and *Ldlr*^{-/-}E06-scFv mice collected after 16 weeks of HCD (*n* = 4 in each group). **e**, Selected list of differentially expressed transcripts in TGEM based on clustering analysis on log₂ ratio reads per kilobase of exon model per million mapped reads (data from **d**). All values represent false discovery rate (FDR)-adjusted values of *P* < 0.05 as described in the Methods. **f**, Aortic wall tissue-resident macrophage phenotypes were determined by FACS analysis of CD45⁺ viable cells. Macrophages were defined as M1-like (CD11b⁺CD11c⁺Arg1⁻) or M2-like (CD11b⁺CD11c⁻Arg1⁺) and expressed as percentage of the frequency of parent (CD11b⁺CD11c^{+/+}) macrophages; *n* = 4 *Ldlr*^{-/-} mice fed with chow; *n* = 4 *Ldlr*^{-/-}E06-scFv mice fed HCD; *n* = 3 *Ldlr*^{-/-} mice fed HCD.

The detailed cellular and molecular mechanisms by which OxPL mediate these proatherogenic and proinflammatory effects are likely to be complex, dependent on the diverse OxPL and different cellular targets involved. For example, OxPL can activate cells by a variety of receptors, including CD36, TLR2–TLR1 and TLR2–TLR6, TLR4, CD14 and combinations of these receptors, and in turn, generate a wide variety of responses^{1,5,7,8,16,22–25}. In addition, the phosphocholine on OxLDL mediates macrophage uptake by CD36 and SR-B1⁵. Presumably, extracellular E06-scFv binds to many of the extracellular OxPL moieties that are formed and by blocking uptake of OxLDL and inhibiting inflammatory signalling, contributes to reduced atherogenesis, although we cannot exclude the possibility that E06-scFv in the intracellular signalling pathway of macrophages or hepatocytes may also contribute in some manner.

In summary, we present a mouse model that demonstrates that, in the context of hypercholesterolemia, OxPL are involved in the pathogenesis of inflammation in general, and atherosclerosis, calcific aortic

valve disease and hepatic steatosis specifically. Calcific aortic valve disease is a growing problem in our ageing population and leads to symptomatic aortic stenosis requiring aortic valve replacement by surgical or transaortic valve approaches in more than 2% of people over the age of 65²⁶. Similarly, OxPL may be involved in the pathogenesis of NASH, which currently afflicts a high percentage of the population and increases the risk for cirrhosis and cardiovascular disease. The E06-scFv transgenic mice can be used to study the mechanisms by which OxPL contributes to these disease processes in vivo, as well as other disease states in which OxPL may have a role. For example, we recently demonstrated with these mice that OxPL restrain bone formation in mice fed either a Western or chow diet²⁷.

This unique sensitivity of E06 to molecules with abnormally presented phosphocholine may allow specific therapeutic targeting of diseased tissues but not normal tissues in a variety of inflammatory states. As shown here as proof-of-principle, diseases of systemic inflammation that generate OxPL may be targets of OxPL-directed therapies. Furthermore,

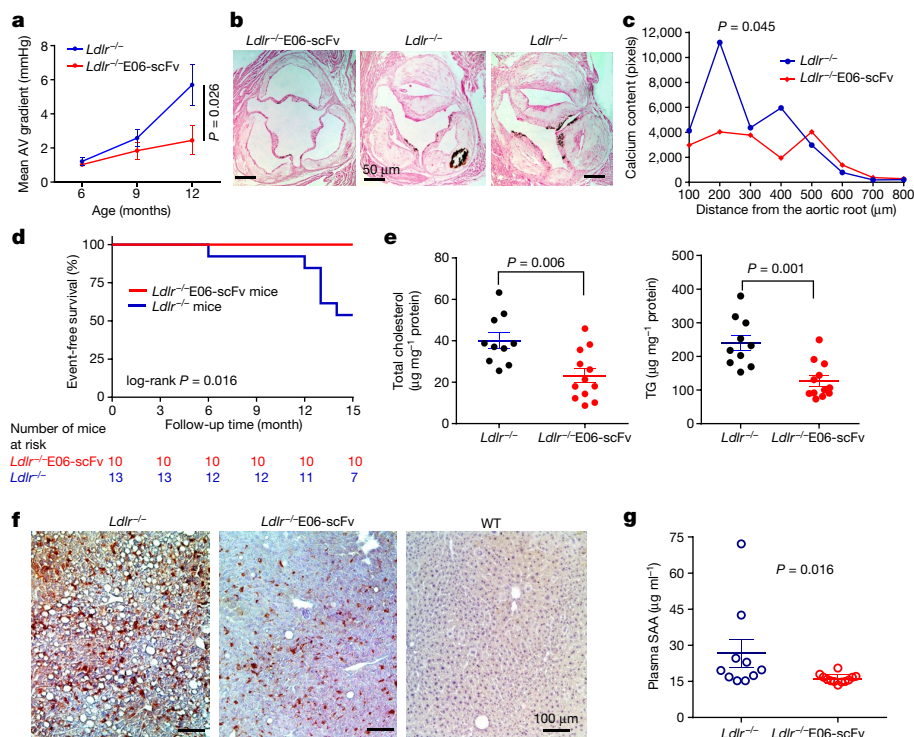


Fig. 4 | E06-scFv decreases early aortic valve stenosis, hepatic steatosis and systemic inflammation. **a, b**, $Ldlr^{-/-}$ ($n = 11$) and $Ldlr^{-/-}$ E06-scFv ($n = 10$) mice were fed a HCD for 15 months and prospectively examined at three time points for aortic valve (AV) haemodynamics. **a**, Mean pressure gradients across the aortic valve, determined by Doppler echocardiography. At 12 months there was a 49% lower mean gradient in the $Ldlr^{-/-}$ E06-scFv mice (2.4 ± 1.9 mmHg (mean \pm s.d.) compared to 4.8 ± 2.4 mmHg; $P = 0.026$). $n = 10$ $Ldlr^{-/-}$ E06-scFv and $n = 9$ $Ldlr^{-/-}$ mice. **b**, Calcification in aortic valve leaflets was determined by von Kossa staining of serial aortic valve sections (black stained areas in sections shown in **b**) and the area under the curves of calcium staining was compared between genotypes. Aortic valve calcium was reduced

in $Ldlr^{-/-}$ E06-scFv mice by 41.5%. $P = 0.045$, one-tailed t -test; $n = 9$ $Ldlr^{-/-}$ E06-scFv and $n = 8$ $Ldlr^{-/-}$ mice. **e**, Survival of mice used in aortic valve haemodynamic study over 15 months. **f**, Hepatic cholesterol and triglyceride (TG) levels were reduced by 42% and 47%, respectively, in $Ldlr^{-/-}$ E06-scFv mice. $n = 10$ $Ldlr^{-/-}$ and $n = 12$ $Ldlr^{-/-}$ E06-scFv mice. **g**, Livers of mice fed a HCD for 16 weeks were immunostained with biotinylated E06 IgM (brown) and compared to chow-fed C57BL/6 (wild-type) mice. Shown are representative photomicrographs, representative of 7 $Ldlr^{-/-}$, 7 $Ldlr^{-/-}$ E06-scFv and 3 wild-type (C57BL/6) mice. **h**, Plasma serum amyloid A (SAA) was decreased by 32% in HCD-fed $Ldlr^{-/-}$ E06-scFv mice. $n = 10$ $Ldlr^{-/-}$ and $n = 12$ $Ldlr^{-/-}$ E06-scFv mice.

OxPL in various tissues can be imaged with OxPL-specific antibodies, such as in atherosclerotic aortas using magnetic resonance imaging-based nanoparticles²⁸, which could aid in the appropriate selection of high-risk patients. The E06-scFv expressed in these mice lacks the Fc effector functions of antibodies, and therefore, its impact was caused solely by blocking biological effects of OxPL. Translational applications of E06 or similar anti-OxPL antibodies to humans, as well as antibodies to other oxidation-specific epitopes^{29,30}, in which more traditional IgG isotypes are more likely to be used, will need to decipher any potential additional roles of various Fc effector functions.

Online content

Any Methods, including any statements of data availability and Nature Research reporting summaries, along with any additional references and Source Data files, are available in the online version of the paper at <https://doi.org/10.1038/s41586-018-0198-8>

Received: 25 July 2017; Accepted: 18 April 2018;
Published online 6 June 2018.

- Binder, C. J., Papac-Milicevic, N. & Witztum, J. L. Innate sensing of oxidation-specific epitopes in health and disease. *Nat. Rev. Immunol.* **16**, 485–497 (2016).
- Shaw, P. X. et al. Natural antibodies with the T15 idiotype may act in atherosclerosis, apoptotic clearance, and protective immunity. *J. Clin. Invest.* **105**, 1731–1740 (2000).
- Friedman, P., Horkko, S., Steinberg, D., Witztum, J. L. & Dennis, E. A. Correlation of antiphospholipid antibody recognition with the structure of synthetic oxidized phospholipids: importance of Schiff base formation and aldol condensation. *J. Biol. Chem.* **277**, 7010–7020 (2002).
- Chang, M. K. et al. Apoptotic cells with oxidation-specific epitopes are immunogenic and proinflammatory. *J. Exp. Med.* **200**, 1359–1370 (2004).
- Miller, Y. I. et al. Oxidation-specific epitopes are danger-associated molecular patterns recognized by pattern recognition receptors of innate immunity. *Circ. Res.* **108**, 235–248 (2011).
- Tsiantoulas, D. et al. Circulating microparticles carry oxidation-specific epitopes and are recognized by natural IgM antibodies. *J. Lipid Res.* **56**, 440–448 (2015).
- Lee, S. et al. Role of phospholipid oxidation products in atherosclerosis. *Circ. Res.* **111**, 778–799 (2012).
- Imai, Y. et al. Identification of oxidative stress and Toll-like receptor 4 signaling as a key pathway of acute lung injury. *Cell* **133**, 235–249 (2008).
- Baldan, A. et al. ABCG1 is required for pulmonary B-1 B cell and natural antibody homeostasis. *J. Immunol.* **193**, 5637–5648 (2014).
- Haider, L. et al. Oxidative damage in multiple sclerosis lesions. *Brain* **134**, 1914–1924 (2011).
- Liu, B. et al. Oxidized phospholipid oxPAPC activates TRPA1 and contributes to chronic inflammatory pain in mice. *PLoS ONE* **11**, e0165200 (2016).
- Oehler, B. et al. Inflammatory pain control by blocking oxidized phospholipid-mediated TRP channel activation. *Sci. Rep.* **7**, 5447 (2017).
- Ikura, Y. et al. Localization of oxidized phosphatidylcholine in nonalcoholic fatty liver disease: impact on disease progression. *Hepatology* **43**, 506–514 (2006).
- Tsimikas, S. A test in context: lipoprotein(a): diagnosis, prognosis, controversies, and emerging therapies. *J. Am. Coll. Cardiol.* **69**, 692–711 (2017).
- Turner, W. W. et al. Design and synthesis of a stable oxidized phospholipid mimic with specific binding recognition for macrophage scavenger receptors. *J. Med. Chem.* **55**, 8178–8182 (2012).
- Seimon, T. A. et al. Atherogenic lipids and lipoproteins trigger CD36-TLR2-dependent apoptosis in macrophages undergoing endoplasmic reticulum stress. *Cell Metab.* **12**, 467–482 (2010).
- Laffitte, B. A. et al. LXRs control lipid-inducible expression of the apolipoprotein E gene in macrophages and adipocytes. *Proc. Natl Acad. Sci. USA* **98**, 507–512 (2001).
- Spann, N. J. et al. Regulated accumulation of desmosterol integrates macrophage lipid metabolism and inflammatory responses. *Cell* **151**, 138–152 (2012).
- Kamstrup, P. R., Hung, M.-Y., Witztum, J. L., Tsimikas, S. & Nordestgaard, B. G. Oxidized phospholipids and risk of calcific aortic valve disease: the Copenhagen general population study. *Arterioscler. Thromb. Vasc. Biol.* **37**, 1570–1578 (2017).

20. Houben, T. et al. Blood-derived macrophages prone to accumulate lysosomal lipids trigger OxLDL-dependent murine hepatic inflammation. *Sci. Rep.* **7**, 12550 (2017).
21. Lewis, K. E. et al. Increase in serum amyloid A evoked by dietary cholesterol is associated with increased atherosclerosis in mice. *Circulation* **110**, 540–545 (2004).
22. Papat, R. J. et al. Anti-myeloperoxidase antibodies attenuate the monocyte response to LPS and shape macrophage development. *JCI Insight* **2**, e87379 (2017).
23. Zononi, I., Tan, Y., Di Gioia, M., Springstead, J. R. & Kagan, J. C. By capturing inflammatory lipids released from dying cells, the receptor CD14 induces inflammasome-dependent phagocyte hyperactivation. *Immunity* **47**, 697–709 (2017).
24. Podrez, E. A. et al. Identification of a novel family of oxidized phospholipids that serve as ligands for the macrophage scavenger receptor CD36. *J. Biol. Chem.* **277**, 38503–38516 (2002).
25. Kadl, A. et al. Oxidized phospholipid-induced inflammation is mediated by Toll-like receptor 2. *Free Radic. Biol. Med.* **51**, 1903–1909 (2011).
26. Towler, D. A. Molecular and cellular aspects of calcific aortic valve disease. *Circ. Res.* **113**, 198–208 (2013).
27. Ambrogini, E. et al. Oxidation-specific epitopes restrain bone formation. *Nat. Commun.* <https://doi.org/10.1038/s41467-018-04047-5> (2018).
28. Briley-Saebo, K., Yeang, C., Witztum, J. L. & Tsimikas, S. Imaging of oxidation-specific epitopes with targeted nanoparticles to detect high-risk atherosclerotic lesions: progress and future directions. *J. Cardiovasc. Transl. Res.* **7**, 719–736 (2014).
29. Tsimikas, S. et al. Human oxidation-specific antibodies reduce foam cell formation and atherosclerosis progression. *J. Am. Coll. Cardiol.* **58**, 1715–1727 (2011).
30. Senders, M. L. et al. PET/MR imaging of malondialdehyde-acetaldehyde epitopes with a human antibody detects clinically relevant atherothrombosis. *J. Am. Coll. Cardiol.* **71**, 321–335 (2018).

Acknowledgements This work was supported by NIH Grants: HL088093 (X.Q., S.T., C.K.G., K.L., Y.I.M. and J.L.W.), HL086559 (J.L.W.), HL119828 (J.L.W. and

S.T.), HL055798 (S.T., J.L.W., Y.I.M., K.L. and C.C.H.), HL136275 (S.T., J.L.W. and Y.I.M.), R35 HL135737 (J.L.W. and Y.I.M.), HL055798 and HL112276 (C.C.H.), HL20948 (J.G.M.), DRC P30 DK063491 (P.L.M.), P42 ES010337 (P.L.M.), P30 CA23100 (P.L.M.), Center for Human Nutrition grant 550015400 (J.G.M.) and Leducq Foundation Transatlantic Grants to J.L.W. and C.K.G. X.Q. was supported in part by a Grant-in-Aid from American Heart Association and D.E.G. was supported in part by an American Heart Association post-doctoral grant (13POST16990031).

Reviewer information *Nature* thanks N. Leitinger, A. R. Tall and the other anonymous reviewer(s) for their contribution to the peer review of this work.

Author contributions X.Q., S.T. and J.L.W. designed the project; X.Q., A.G., T.A.P., X.S., C.D., A.M., D.E.G., K.B., J.P. and J.G.M. conducted key experiments; P.L.M., C.C.H., K.L., K.L.P. and C.K.G. provided vital technical expertise and advice; M-Y.H., C.Y., K.L.P. and S.T. conducted aortic valve studies; X.Q. and J.L.W. wrote the manuscript with expert input from C.K.G., Y.I.M., S.Y-H., C.J.B., S.T. and all other coauthors.

Competing interests X.Q., S.T. and J.L.W. are co-inventors and receive royalties from patents owned by the University of California San Diego on the use of oxidation-specific antibodies. S.T. currently has a dual appointment at UCSD and as an employee of Ionis Pharmaceuticals. J.L.W. is a consultant to Ionis Pharmaceuticals.

Additional information

Extended data is available for this paper at <https://doi.org/10.1038/s41586-018-0198-8>.

Supplementary information is available for this paper at <https://doi.org/10.1038/s41586-018-0198-8>.

Reprints and permissions information is available at <http://www.nature.com/reprints>.

Correspondence and requests for materials should be addressed to J.L.W.
Publisher's note: Springer Nature remains neutral with regard to jurisdictional claims in published maps and institutional affiliations.

METHODS

Antigen preparation and modifications. Plasma was obtained from healthy donors after an overnight fast following consent under a protocol approved by the UCSD Human Research Protections Program. LDL was isolated by sequential ultracentrifugation, and modified with malondialdehyde (MDA), malondialdehyde-acetaldehyde adducts (MAA) or CuSO_4 to generate MDA-LDL, MAA-LDL or copper-oxidized LDL (Cu-OxLDL), respectively, as previously described³¹. Phosphocholine-BSA (PC-BSA) was from Biosearch Technologies and POVPC-BSA was prepared as described³². Monoclonal anti-Myc and anti-His alkaline phosphatase-conjugated antibodies were from Sigma-Aldrich.

E06-scFv construction and optimized expression. In the Supplementary Information, we describe in detail the history of the discovery of the IgM natural antibody E06/T15 and its binding specificity and biological properties. The cDNAs encoding the E06 variable heavy and light regions were connected with an oligo linker peptide of 15-amino acids (Gly_4Ser)₃ that were assembled by overlapping PCR and cloned into an expression vector (pSecTag2A (Invitrogen)), which contains a mouse Ig κ -chain leader sequence for secretion and Myc and polyHis tags that facilitates purification and detection. HEK293 cells (obtained from ATCC, mycoplasma not tested recently) were transfected with the pSecTag2A-E06-scFv plasmid using Lipofectamine plus (Invitrogen). Stable transfectants were selected with zeocin, and the E06-scFv antibody in the culture supernatant was identified using an ELISA plate pre-coated with Cu-OxLDL or PC-BSA and detection by anti-Myc or anti-His tag antibody conjugate using chemiluminescent assay techniques described previously²⁹. During development, multiple linkers were tried and in addition, site-directed mutagenesis in framework region 1 was performed at seven sites in an iterative fashion using a QuickChange Multi Site-Directed Mutagenesis Kit (Stratagene) to create point mutations to improve the folding, stability, yield and reduce the aggregation of recombinant scFv. His6-tagged E06-scFv was purified on Ni-NTA agarose beads (Qiagen) according to the manufacturer's protocols. In brief, cell lysates were clarified by centrifugation (20,000g, 30 min, 4 °C), and the supernatant applied to a Ni²⁺-NTA agarose column, from which His6-tagged E06-scFv was eluted with 250 mM imidazole. Fractions containing E06-scFv were pooled and extensively dialysed against PBS before use. The purity and integrity were assessed by SDS-PAGE and western blot with anti-His6-tag antibody-HRP conjugate, and an ECL detection system (Amersham).

Generation of E06-scFv transgenic mice. The liver-specific expression vector pLiv7 was used to generate transgenic mice expressing the E06-scFv transgene driven by the *Apoe* promoter, as previously reported³³. The MfeI-MluI fragment from the pSecTag2A-E06-scFv plasmid including the mouse Ig κ leader sequence and Myc/His tags was released by MfeI and MluI digestion, and inserted into the polylinker region of pLiv7 to generate a transgenic vector pLiv7-E06-scFv. The *Apoe*-E06-scFv transgene consists of 3.0-kb *Apoe* promoter + N-terminal UTR of *Apoe* gene + E06-scFv transgene + C-terminal UTR of *Apoe* gene and a 0.77-kb hepatic control element (LE6) placed downstream of poly(A) signal (Fig. 1). To create transgenic mice, a 6.8-kb *Apoe*-E06-scFv transgene cassette was separated from the vector by digestion with SacII and SpeI, purified, and injected into the pronuclei of fertilized mouse eggs obtained from superovulated female mice (C57BL/6). The injected eggs were surgically transferred to oviducts of surrogate C57BL/6 females in the UCSD Transgenic and Knockout Mouse Core.

Production and screening of transgenic mice. Offspring were screened for plasma E06-scFv titre and integration of the transgene by PCR amplification of the tail DNA with the upstream primer sequence MfeFw 5'-TACAATTGAGCTGGCTAGCCACCATGGAG-3' and the downstream E06Rev3 primer sequence 5'-GCTGTACCAAGCCTCCTCCAGACTCCACCAG-3' to yield a 540-bp product corresponding to the nucleotide sequence between -15 and 525 of E06-scFv cDNA. Mice from the highest expressing transgenic E06-scFv founder lines were bred with each other to generate 'homozygous' transgenic mice, and in turn, these were crossed into *Ldlr*^{-/-} and *Ldlr*^{-/-}*Rag1*^{-/-} mice, all on the C57BL/6 background. All animals were genotyped for E06-scFv and *Ldlr*^{-/-} and plasma assayed to confirm expression of the E06-scFv by immunoassay.

Binding profile of plasma E06-scFv quantified by chemiluminescent ELISA. E06-scFv plasma titres were determined by chemiluminescent ELISA assays for binding to phosphocholine epitopes as expressed on Cu-OxLDL, phosphocholine-KLH, PC-BSA, POVPC-BSA, and capsular polysaccharide (C-PS) of *Streptococcus pneumoniae*, as well as to the anti-T15 idiotypic antibody AB1-2². Competition immunoassays were performed to demonstrate specificity^{31,32}. In brief, 96-well round-bottom MicroFluor plates (DYNEX Technologies) were coated with various antigens at 5 $\mu\text{g ml}^{-1}$ (50 μl per well) in PBS overnight at 4 °C. After the plates were washed and blocked with 1% BSA in Tris-buffered saline (TBS) for 30 min, 25 μl of primary antibodies diluted with 1% BSA in PBS were added to the wells, in the absence or presence of competitors and incubated for 90 min at room temperature. Bound antibodies were detected with anti-His6-tag antibody conjugated to alkaline phosphatase (Sigma-Aldrich), in TBS buffer containing 1% BSA, followed by a rinse with water and the addition of 25 μl of 50% LumiPhos

530 (Lumigen) as luminescent substrate. The light emissions were measured, and counts expressed as relative light units over 100 ms using a Dynex Luminometer (DYNEX Technologies). For competition immunoassays, data are expressed as B/B₀, where B represents binding in presence and B₀ in absence of competitors. In separate experiments, the absolute plasma E06-scFv levels in transgenic mice were determined using a standard curve generated with purified His6-tagged E06-scFv isolated as described above. All determinations were done in triplicate.

Flow cytometry and deconvolution microscopy of E06-scFv mouse plasma binding to apoptotic cells. Plasma of *Ldlr*^{-/-}E06-scFv and *Ldlr*^{-/-} control mice were analysed for binding to apoptotic cells by flow cytometry (FACS) analysis as described⁴. Thymocytes collected from C57BL/6 mice were cultured in cell culture medium and induced to undergo apoptosis by 10 ng ml⁻¹ PMA (Sigma-Aldrich) for 16 h. Plasmas diluted in 1% BSA in PBS were incubated with apoptotic thymocytes for 1 h at 4 °C, followed by incubation with a FITC-labelled anti-His6 monoclonal antibody in 1% BSA in PBS for 30 min at 4 °C. Apoptotic cells were double-stained with annexin V-phycoerythrin (annexin V-PE) and 7-amino-actinomycin (7AAD) (BD Biosciences) for 15 min and immediately analysed by FACS using a FACSCanto (BD Biosciences). For immunofluorescence microscopy studies, apoptotic Jurkat cells were prepared by exposure to UV irradiation at 20 mJ cm⁻², and further cultured for 16 h before use. Apoptotic Jurkat cells (from ATCC, mycoplasma not tested recently) were incubated with 100 μl of plasma (1:20) in 1% BSA in PBS at 4 °C for 1 h, washed and labelled with a FITC-conjugated anti-His6-tag monoclonal antibody (1:1,000) and 1 $\mu\text{g ml}^{-1}$ of Hoechst dye (Sigma-Aldrich) for 45 min at 4 °C. The cells were fixed with 3.7% paraformaldehyde for 20 min, washed and resuspended in 1% BSA in PBS. The cells were spun down on glass slides using cytospin (Thermo Shandon). Images were captured using a DeltaVision deconvolution microscopic system operated by SoftWorx software (Applied Precision).

Demonstration of specificity of E06-scFv binding to OxPL and ability to inhibit OxLDL binding to macrophages. Binding of biotinylated OxLDL to J774 macrophages plated in microtitre wells was assessed by a chemiluminescent binding assay as described recently³⁴. In brief, biotinylated Cu-OxLDL (5 $\mu\text{g ml}^{-1}$) was incubated overnight in the absence or presence of E06-scFv-Tg plasma or control at various dilutions at 4 °C. The supernatants were then added to macrophages plated in 96-well microtitre plates and the binding of biotinylated OxLDL detected by alkaline phosphatase-labelled NeutrAvidin and chemiluminescent ELISA.

Effect of E06-scFv on atherosclerosis in *Ldlr*^{-/-} mice. Animal protocols were approved by the Institutional Animal Care and Use Committee (IACUC) at University of California San Diego. At 8 weeks of age, 18–20-g male *Ldlr*^{-/-} or *Ldlr*^{-/-}E06-scFv mice were matched for age, body weight and total cholesterol and placed on a 1% cholesterol diet (HCD) (TD97131, Harlan Teklad) to determine the effect of the E06-scFv on progression of atherosclerosis. For each study, we sought to have 8–10 mice per group, which based on experience would be sufficient to detect differences in atherosclerosis. The identity of the mice was not blinded during the HCD feeding period, but determination of atherosclerosis, the outcome of the study, was done in a blinded fashion. Blood samples were collected from submandibular bleeding at time 0, and various time points on diet. Mice were weighed monthly, and total cholesterol and triglycerides levels were determined using automated enzymatic assays (Roche Diagnostics, Indianapolis). Lipoprotein profiling was performed on terminal blood samples using fast performance liquid chromatography equipped with a Superose 6 column, and total cholesterol and triglycerides levels in each fraction were determined as previously described²⁹.

Bone marrow transplantation study. Bone marrow transplantation (BMT) was performed as previously described³⁵. In brief, bone marrow was collected from cleaned femurs and tibias of male E06-scFv mice (not on a *Ldlr*^{-/-} background) and wild-type C57BL/6 mice and re-suspended in RPMI 1640 medium for injection. *Ldlr*^{-/-} male recipient mice were fasted overnight and received a lethal dose of radiation (9 Gy) 4 h before bone marrow injection. Mice ($n = 13$ per group) were anaesthetized with isoflurane, and 5×10^6 bone marrow cells either from E06-scFv mice or from C57BL/6 wild-type mice were injected into the retro-orbital venous plexus. Three days before and two weeks after the BMT, recipient mice received autoclaved acidified (pH 2.7) water supplemented with 100 $\mu\text{g ml}^{-1}$ neomycin and 10 $\mu\text{g ml}^{-1}$ polymyxin B sulphate. Two weeks after BMT, all mice were given a Western diet (TD00457, Harlan) for 16 weeks to induce atherosclerosis. Reconstitution of transplanted bone marrow was confirmed based on titres of E06-scFv secretion in plasma.

Atherosclerosis analysis. Mice exposed to a HCD or Western diet were euthanized using 100% CO₂. Sections of spleen, kidney and liver tissues were frozen in RNAlater solution (Ambion) for mRNA extraction or embedded in OCT (Sakura Tissue-Tek) for cryosectioning. After perfusion with 4% formalin-sucrose for 15 min, livers and hearts were removed, fixed and embedded in paraffin and serially sectioned. The aortas were dissected under a microscope and fixed in 4% formalin-sucrose, opened, flattened pinned and stained with Sudan IV, and images of the aortas were captured and quantified by analysis of the entire en face aorta

as previously described³⁵. Aortic root cross-sectional lesion areas were quantified using serial cross-sections taken at 100- μ m intervals between 100 μ m and 900 μ m beginning with the first appearance of the first leaflet of the aortic valve until the last leaflet. Mean lesion size at each 100- μ m section in each animal was determined by computer-assisted morphometry (Image-Pro Plus 6.3, Media Cybernetics) on serial 10- μ m paraffin sections. Modified van Gieson elastic stain was used to enhance the contrast between the intima and surrounding tissue. Cross-sectional plaque area and plaque morphology were evaluated by two investigators blinded to the study protocol. The results are presented as mean of all values for each interval plotted versus the distance from first leaflet and the overall extent of aortic root lesions was determined by area under the curve (AUC) analysis of all serial sections in each group.

In lesions of the four-month HCD experiments, we also determined the area of necrosis by computer-assisted morphometric analysis of extent of necrosis of five lesions taken at each 100- μ m interval and expressed as the absolute area involved at that site. In the seven-month experiment, lesions on each of the 100- μ m sections were selected to be of equal total size between the *Ldlr*^{-/-} and *Ldlr*^{-/-}E06-scFv aortic sections at that level, and the area of necrosis determined and plotted at each 100- μ m section. For both the four- and seven-month analyses, the extent of necrotic area was determined as the AUC analysis of all serial sections in each group.

Echocardiographic and histological analysis of aortic valve. *Ldlr*^{-/-} ($n = 13$) and *Ldlr*^{-/-}E06-scFv ($n = 10$) mice were fed a HCD for 15 months and aortic valve function was serially evaluated with Doppler ultrasound, 2D and M-mode echocardiography at 6, 9 and 12 months. At 15 months, the extent of atherosclerosis was determined and aortic valves evaluated histologically. A Kaplan–Meier survival analysis was also performed on the entire cohort. Severity of aortic sclerosis was determined quantitatively by calculating peak pressure gradients across the aortic valves using Doppler analysis and measurement of aortic valve leaflet thickness using M-mode echocardiography. Pressure gradients were determined from aortic blood flow velocities (V) using the principles of conservation of energy and calculated by the modified Bernoulli equation ($\Delta P = 4(V_{\text{aorta}}^2 - V_{\text{LVOT}}^2)$)⁹. Images were acquired using high-resolution (32–55 MHz) ultrasound (VisualSonics Vevo 2100) as previously described³⁶. Histological assessment of aortic valves was determined on serial sections at 100- μ m intervals from the origins of the aortic valve leaflets at the base of the aortic root, and stained for calcium using Von Kossa's method. Calcium on each section was quantified by number of pixels 'stained' using ImageJ software. Total aortic valve calcium was determined by AUC analysis of all serial sections in each group.

Immunohistochemical analyses of atherosclerotic lesions and liver tissues. Immunohistochemical studies were performed on sections of paraformaldehyde-fixed and paraffin-embedded tissues. Paraffin sections of atherosclerotic lesions, aortic roots and liver tissues were stained for OxPL with biotinylated E06 IgM, or with E06-scFv using a biotinylated monoclonal antibody anti-Myc tag (Miltenyi Biotec) following the manufacturer's instructions. Endogenous peroxidase activity was blocked with 0.3% hydrogen peroxide in PBS for 15 min. After blocking, non-specific binding sites with 10% normal goat serum and Fc Block (2.4G2 antibody) in PBS for 30 min, slides were incubated with primary antibodies for 1 h at room temperature. Biotinylated antibodies (E06, anti-Myc and anti-polyHis) were revealed with ABC-HRP VectaStain kit (Vector Laboratories, Burlingame, California) and/or NovaRed substrate (Vector Labs). Slides were counterstained by haematoxylin and in some experiments, percentage of positively stained targets were quantified by image analysis morphometry (Image-Pro Plus).

Determination of cellular composition of aorta. Cellular composition of aortas was determined in the Cell Phenotyping Core of the UCSD PPG on Role of Immune Mechanisms in Inflammation and Atherosclerosis, under the direction of K.L., using established techniques³⁷. In brief, six aortas from 16-week chow-fed *Ldlr*^{-/-}, six from HFD-fed *Ldlr*^{-/-} and five from *Ldlr*^{-/-}E06-scFv mice were dissected following heparin PBS perfusion and adventitia were carefully removed. The intact aortas were incubated for 1 h with an Aorta Dissociation Enzyme stock solution and single-cell suspensions were prepared from the digested aorta by shearing the aortas apart and passing cells through a 70- μ m cell strainer into 5-ml polypropylene FACS tubes (BD Falcon). The cells were pelleted by centrifugation (400g, 5 min, 4 °C), resuspended in 1 ml of FACS buffer (PBS supplemented with 1% BSA and 0.05% NaN₃), counted and assessed for viability using trypan blue in a haemocytometer. Cells were stained on ice for 30 min with the panel of antibodies below, washed twice with FACS buffer and then analysed at La Jolla Institute for Allergy and Immunology using a FACSAria analyser. Anti-CD45 antibody and fixable live-dead cell stain (Invitrogen, Molecular Probes) was added to all samples to allow for gating of live CD45⁺ leukocytes and cells were sorted with the panel of antibodies listed in in Supplementary Table 1.

Analysis of T cells in blood, spleen and periaortic lymph nodes by flow cytometry. Blood from *Ldlr*^{-/-} or *Ldlr*^{-/-}E06-scFv mice was collected in 4% sodium citrate solution. Blood lymphocytes were obtained from the interface after

underlying and spinning the blood with Histopaque 1077 (Sigma-Aldrich). Periaortic lymph nodes and spleens were processed to obtain single-cell suspensions. Spleen samples were lysed with 1 \times RBC lysis buffer (BioLegend). Cell suspensions were counted using a Z2 Coulter counter (Beckman Coulter) to obtain absolute numbers of each cell population. Single-cell suspensions were stained as routinely done in our laboratory³⁸, with antibodies against CD4 (clone RM4-5; Life Technologies), CD8 (clone 53-6.7; Biolegend), TCR β (periaortic LNs and spleen only) (clone H57-597; eBioscience), CD44 (clone IM7, Biolegend), CD25 (clone PC61, Biolegend) and live/dead exclusion yellow dye (Life Technologies) in FACS buffer (2% BSA in PBS). Cells were stained on ice for 30 min, washed twice with FACS buffer and then samples were analysed using LSRII (BD Bioscience). Data were analysed using FlowJo 9.7 (Tree Star Inc.).

RNA analysis of tissues. Total RNAs were extracted from individual frozen tissue samples (livers) or TGEM using RNeasy mini kit (Qiagen) as per the manufacturer's instructions. Tissues were homogenized in RNeasy lysis buffer with a motorized homogenizer. Genomic DNA was removed by DNase I, and RNA concentration and quality were assessed with by NanoDrop. Next, 1 μ g of RNA was reversely transcribed to cDNA using EcoDry Premix kit (Clontech). Real-time qPCR was carried out to determine gene expression of inflammatory molecules. All reactions were performed in the Rotor-Gene Q cyclor (Qiagen) in triplicates using 50 ng of cDNA and qPCR Master Mix (Eurogentec), primers and Taqman fluorescent probes (Applied Biosystems) in a total reaction volume of 20 μ l. Relative quantities of mRNA were calculated using $\Delta\Delta C_t$ formula and two standard curves relative quantification using Rotor-Gene Q Software 1.7 (Qiagen) with *Gapdh* as the reference gene.

Analyses of peritoneal macrophages. Thioglycollate-elicited peritoneal macrophages (TGEM) from *Ldlr*^{-/-} and *Ldlr*^{-/-}E06-scFv-Tg mice fed a HCD diet for five weeks were isolated three days after intraperitoneal injection of 1 ml of 2% thioglycollate broth (Sigma-Aldrich) as previously described¹³. TGEM were collected for RNA-sequencing analysis, cholesterol analysis and mass spectrometry determinations of sterols as previously described¹⁸. TGEM were isolated from three mice in each group and each set of macrophages divided into two separate aliquots, which were individually extracted and sterols determined in triplicate by liquid chromatography–tandem mass spectrometry following LipidMaps protocols online at <http://www.lipidmaps.org/>.

In other studies to assess the ability of macrophages to secrete the E06-scFv, TGEM were obtained from E06-scFv-Tg mice plated at a density of 5 million cells per well in 6-well plates in 10% FBS in RPMI. On day 4, cells were incubated with T0901317 at 10 μ M ml⁻¹ (or vehicle) in 1% delipidated, charcoal-stripped FBS in RPMI. Cell-culture supernatants were concentrated and assessed for E06-scFv-binding activity by ELISA. Cell pellets were checked for expression of E06-scFv by qPCR.

RNA-sequencing analysis was performed on TGEM from four biological replicates. Total RNAs were converted into cDNA libraries as templates for high-throughput sequencing using Illumina HiScanSQ or HiSeq2500 following the Illumina TruSeq RNA sample preparation protocol. In brief, first-strand cDNA was synthesized from 5 μ g of total RNA using oligo-dT primers and EcoDry Premix kit (Clontech) for cDNA synthesis, and subsequently converted into blunt ends via exonuclease/polymerase. After adenylation of 3' ends of DNA fragments, Illumina PE adapters were ligated to prepare cDNA fragments of preferentially 200 bp in length and enriched using Illumina PCR primers in a 15-cycle PCR reaction. After cluster generation, 100-bp paired-end reads were generated and analysed by alignment to the UCSC mouse reference genome using TopHat/Bowtie. The numbers of reads mapping to exonic and intronic regions as well as to splice sites were calculated based on the UCSC annotation file. Reads per kilobase of exon model per million mapped reads (RPKM) values for Refseq genes were established. RNA-sequencing clusters were analysed by Cuffdiff2, TreeView6, for heat map, and DAVID6.7 to determine differential gene expression (DEG) between *Ldlr*^{-/-} and *Ldlr*^{-/-}E06-scFv macrophages, and by Gene Ontology classification to assign gene changes to different functional categories. For statistical analysis of DEG, the Cufflinks data of P values from the t -tests of RPKM in RNA-sequencing data were further analysed using R packages (DESeq2) from Illumina BaseSpace Sequence Hub and converted to FDR-adjusted Q values. The concise output files included only those transcripts that have a Q value lower than the given FDR, and the value of the significant column was adjusted accordingly (yes/no) in all output files. All DEG values shown are FDR-corrected $P < 0.05$.

Determination of uptake of fluorescent OxLDL by peritoneal macrophages in vivo. *Rag1*^{-/-} mice lack T and B cells and plasma antibodies. *Rag1*^{-/-}*Ldlr*^{-/-} mice and *Rag1*^{-/-}*Ldlr*^{-/-}E06-scFv transgenic mice (which only have E06-scFv antibodies) were injected intraperitoneally with 1 ml of sterile 2% thioglycollate to induce sterile peritonitis. Four days later, the mice were injected intraperitoneally with 100 μ g of AlexaFluor-488-labelled OxLDL in 200 μ l PBS per *Ldlr*^{-/-} mouse³⁹. The mice were euthanized 1 h after injection, and peritoneal cells were recovered by lavage with 10 ml of ice-cold PBS containing 1% heat-inactivated FBS and 10 mM

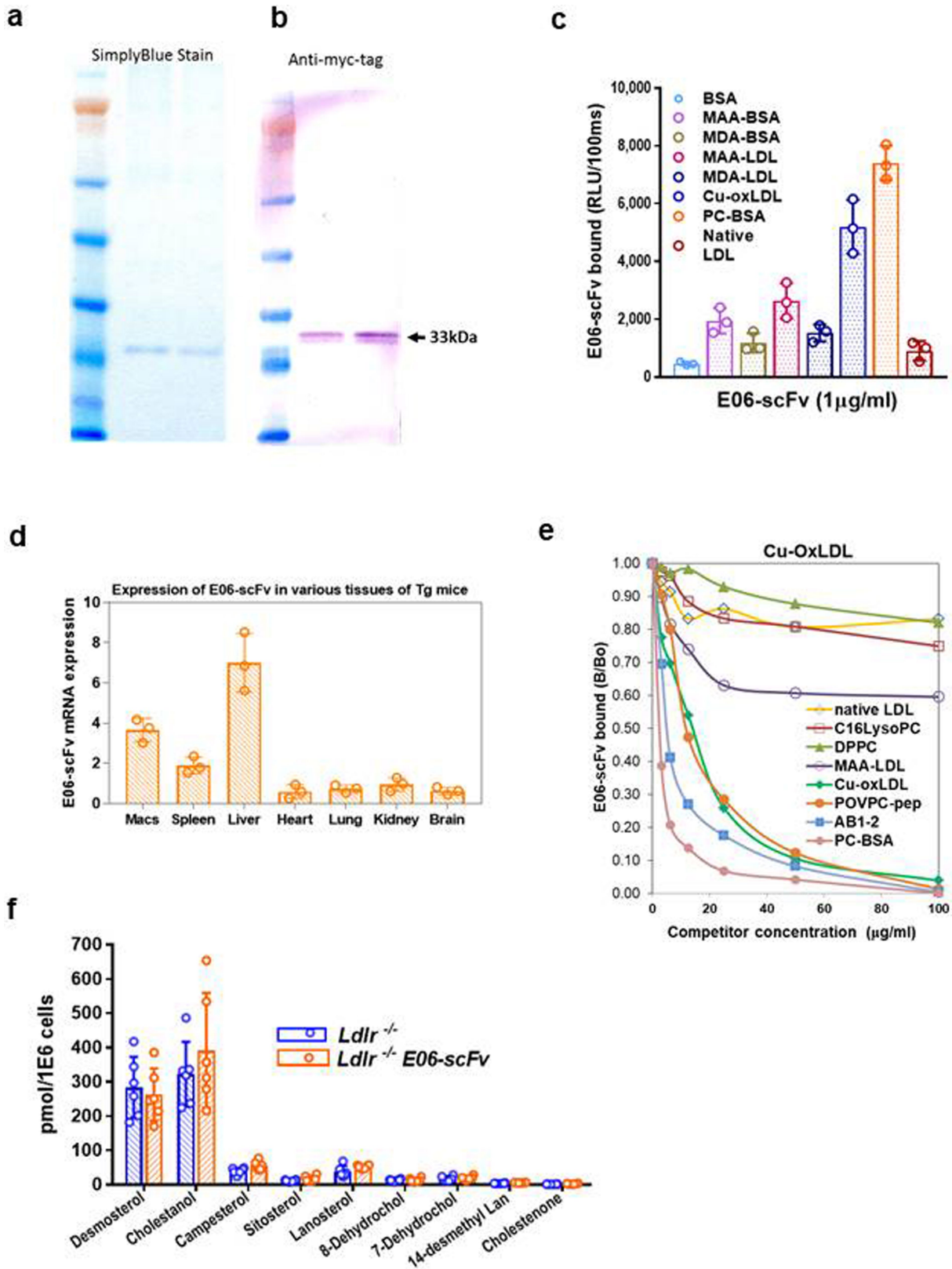
EDTA. Peritoneal macrophages were labelled with anti-F4/80 APC-conjugated monoclonal antibody (eBioscience) and macrophage-specific uptake of OxLDL was analysed by FACS for the presence of intracellular labelled OxLDL. In a separate experiment, AlexaFluor-488-labelled OxLDL was pre-incubated with plasma from *Ldlr*^{-/-}, *Rag1*^{-/-}*Ldlr*^{-/-} or *Rag1*^{-/-}*Ldlr*^{-/-}E06-scFv mice for 1 h, and then injected intraperitoneally into *Ldlr*^{-/-}*Rag1*^{-/-} mice. In both experiments, uptake of OxLDL by elicited peritoneal macrophages in vivo was expressed as the percentage of macrophages ingesting OxLDL.

Statistical analysis. Unless otherwise noted, data are expressed as mean \pm s.e.m. Statistical analysis was performed in GraphPad Prism 7.04 using the two-tailed Student's *t*-test and one-way ANOVA with appropriate post hoc tests as needed. When variances were different, differences between groups were analysed using a nonparametric multiple comparison test. Lesion size, lesion morphology and gene expression were evaluated using the Mann–Whitney *U*-test.

Reporting summary. Further information on experimental design is available in the Nature Research Reporting Summary linked to this paper.

Data availability. The datasets generated during and/or analysed during the current study are available from the corresponding author on reasonable request. The raw sequence data presented in this Letter have been submitted to the NCBI Sequence Read Archive under accession number PRJNA438959.

31. Gonen, A. et al. Atheroprotective immunization with malondialdehyde-modified LDL is hapten specific and dependent on advanced MDA adducts: implications for development of an atheroprotective vaccine. *J. Lipid Res.* **55**, 2137–2155 (2014).
32. Chou, M. Y. et al. Oxidation-specific epitopes are dominant targets of innate natural antibodies in mice and humans. *J. Clin. Invest.* **119**, 1335–1349 (2009).
33. Schneider, M. et al. High-level lipoprotein [a] expression in transgenic mice: evidence for oxidized phospholipids in lipoprotein [a] but not in low density lipoproteins. *J. Lipid Res.* **46**, 769–778 (2005).
34. Montano, E. N. et al. Development and application of a nonradioactive binding assay of oxidized low-density lipoprotein to macrophage scavenger receptors. *J. Lipid Res.* **54**, 3206–3214 (2013).
35. Binder, C. J. et al. IL-5 links adaptive and natural immunity specific for epitopes of oxidized LDL and protects from atherosclerosis. *J. Clin. Invest.* **114**, 427–437 (2004).
36. Cowling, R. T. et al. Discoidin domain receptor 2 germline gene deletion leads to altered heart structure and function in the mouse. *Am. J. Physiol. Heart Circ. Physiol.* **307**, H773–H781 (2014).
37. Butcher, M. J., Herre, M., Ley, K. & Galkina, E. Flow cytometry analysis of immune cells within murine aortas. *J. Vis. Exp.* **53**, e2848 (2011).
38. Nowyhed, H. N. et al. The nuclear receptor Nr4a1 controls CD8 T cell development through transcriptional suppression of Runx3. *Sci. Rep.* **5**, 9059 (2015).
39. Choi, S. H. et al. Lipoprotein accumulation in macrophages via Toll-like receptor-4-dependent fluid phase uptake. *Circ. Res.* **104**, 1355–1363 (2009).



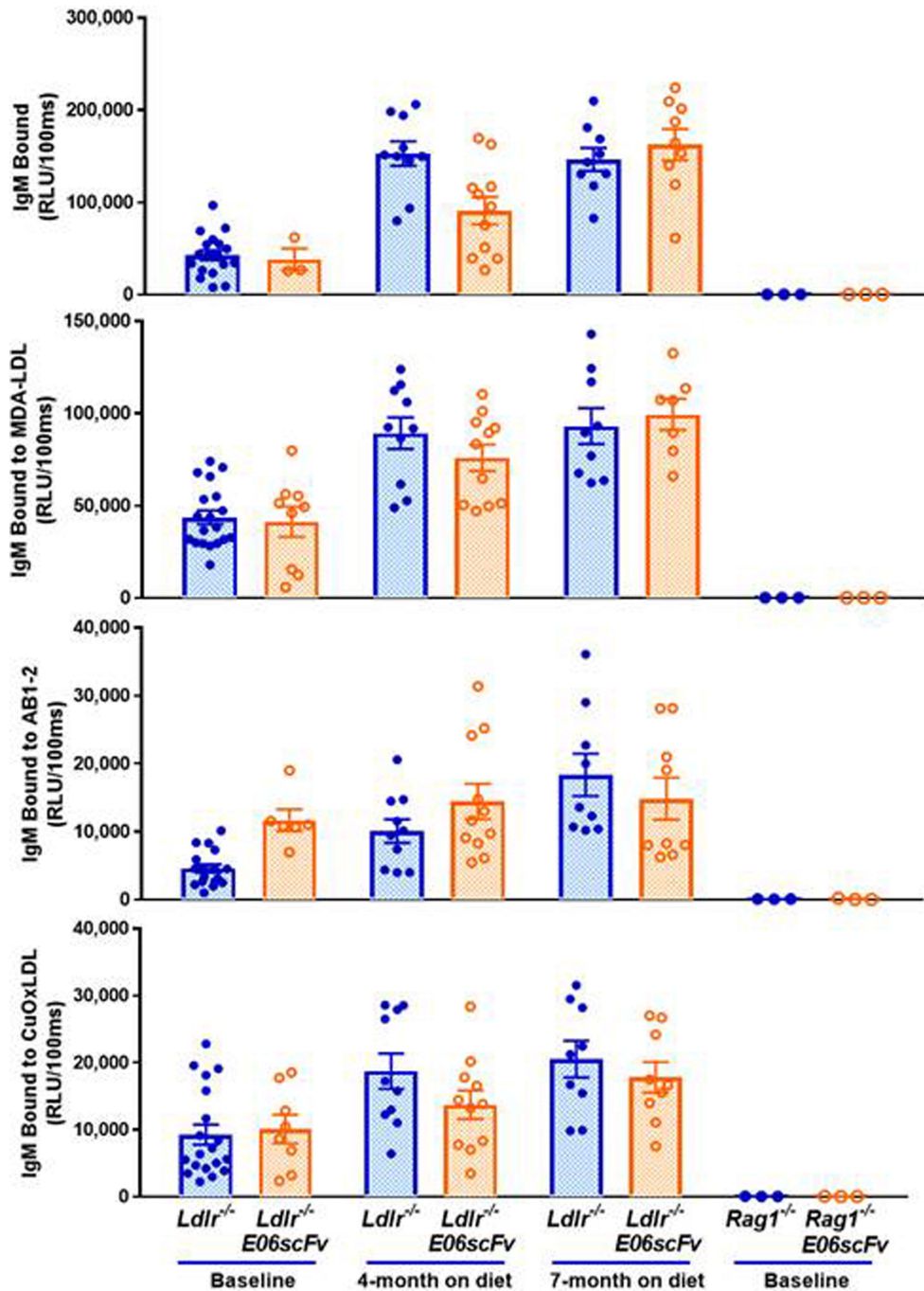
Extended Data Fig. 1 | See next page for caption.

Extended Data Fig. 1 | E06-scFv expression and binding characteristics.

a, Simply blue staining of purified E06-scFv from HEK293 cell lysates from two experiments. **b**, Western blot with anti-Myc antibody of E06-scFv following purification on Ni-NTA agarose beads (representative of four independent experiments). **c**, Binding profile of purified E06-scFv using chemiluminescent ELISA. Binding data are mean \pm s.e.m., using three independent samples, each determined in triplicate.

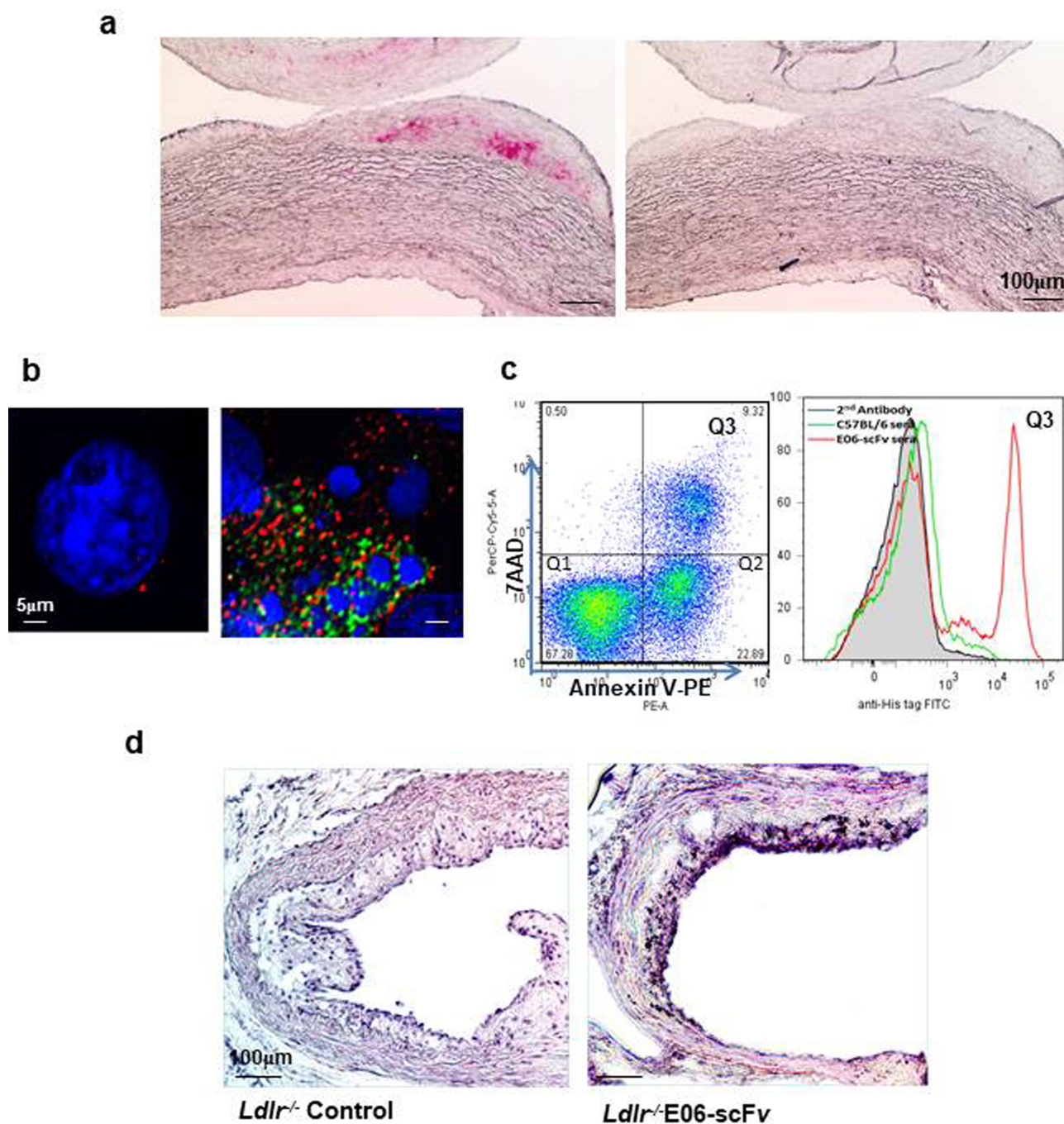
d, Tissue distribution of the E06-scFv gene transcript in *Ldlr*^{-/-}E06-scFv mice determined by qPCR. Data are mean \pm s.e.m., determined from tissues of three *Ldlr*^{-/-}E06-scFv mice. **e**, Competition immunoassays of *Ldlr*^{-/-}E06-scFv plasma binding to plated OxLDL in the presence or

absence of increasing amounts of indicated competitors. Results are the ratios of E06-scFv binding to OxLDL in the presence (B) or absence of a competitor (B₀). AB1-2 is a T15 anti-idiotypic antibody; C₁₆lysoPC, C₁₆ lysophosphatidylcholine; DPPC, dipalmitoyl phosphatidylcholine. Data are triplicates of each point from one competition experiment, representative of four separate studies of similar nature. **f**, Accumulation of desmosterol and other indicated sterols in TGEM from indicated mice fed a HCD for 16 weeks. TGEM were isolated from three mice in each group and each set of macrophages divided into two separate aliquots for analysis in triplicate. Data are mean \pm s.e.m. There were no differences between respective sterol pairs, *P* > 0.05 for all pairs.



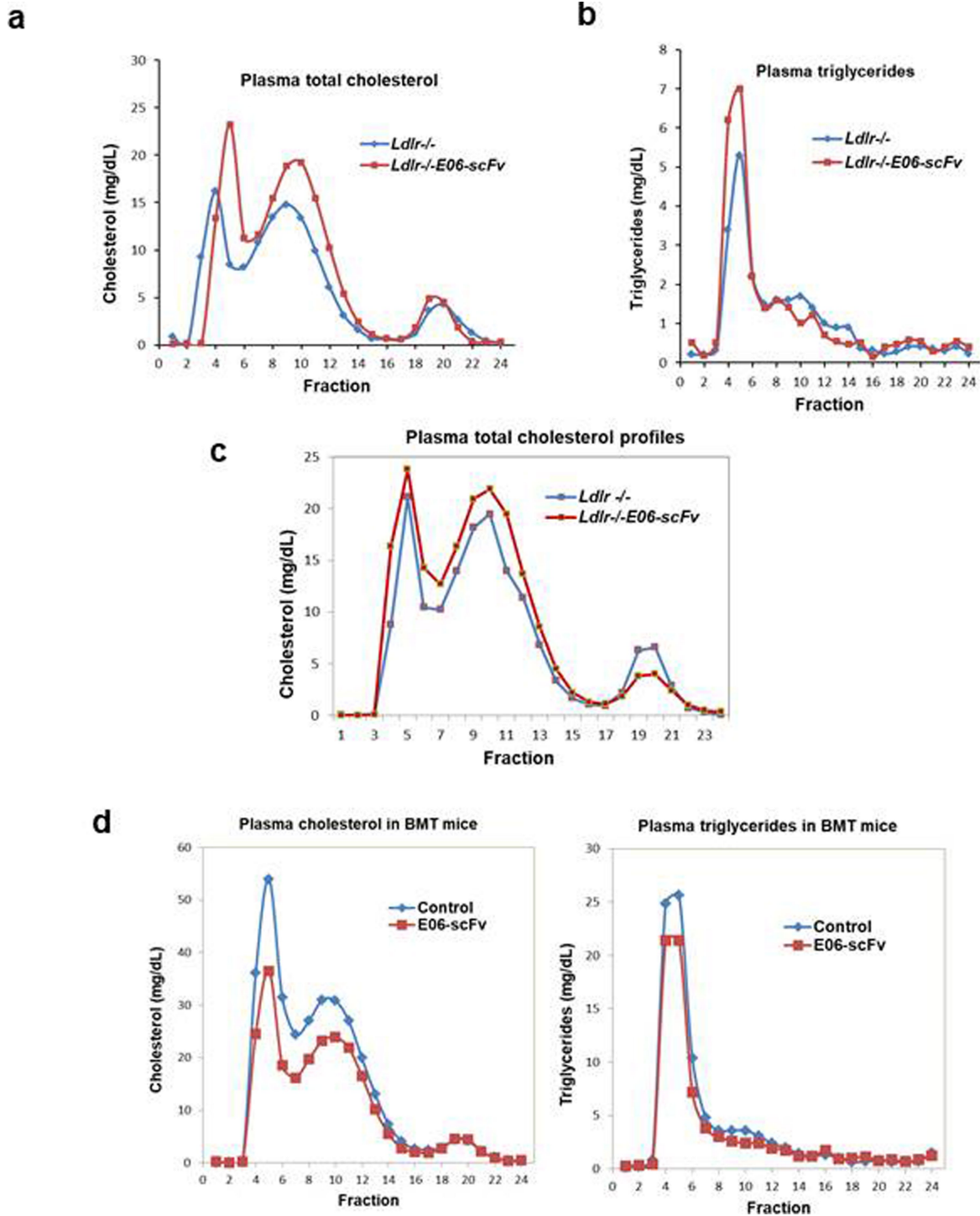
Extended Data Fig. 2 | Expressed E06-scFv does not alter the levels of total IgM or IgM-E06 (detected by AB1-2) in transgenic mice. Comparison of plasma IgM titres to indicated antigens of *Ldlr*^{-/-} or *Ldlr*^{-/-}E06-scFv mice at baseline or after four or seven months of HCD. Note significant increases in total IgM and IgMs against MDA-LDL and OxLDL at four and seven months compared to respective baseline titres (all values, $P < 0.001$) except at four months, at which time the

total IgM of *Ldlr*^{-/-}E06-scFv mice and E06 (detected by AB1-2) in both mouse groups were not different from their respective baselines ($P > 0.05$). Notably, there were no significant differences in any antibody titres between *Ldlr*^{-/-} or *Ldlr*^{-/-}E06-scFv mice at any time point, and in particular, note that endogenous IgM-E06 titres (detected by AB1-2 binding) were similar. As expected, the plasma from *Rag1*^{-/-} and *Rag1*^{-/-}E06-scFv mice did not have any IgM.



Extended Data Fig. 3 | Plasma E06-scFv binds to atherosclerotic lesions and apoptotic thymocytes and is present in the aorta of *Ldlr*^{-/-} E06-scFv mice. **a, Staining of atherosclerotic lesions of Watanabe heritable hyperlipidaemic (WHHL) rabbit aortas with E06-scFv plasma (left) and plasma from *Ldlr*^{-/-} mice (right) (both at dilution of 1:20), visualized using a biotinylated anti-Myc monoclonal antibody and ABC-AP VectaStain kit. **b**, Deconvolution microscopy of E06-scFv plasma (1:20 dilution) binding to apoptotic but not normal cells. Blue, nuclei stained with Hoechst; green, FITC-labelled anti-His6-tag monoclonal antibody;**

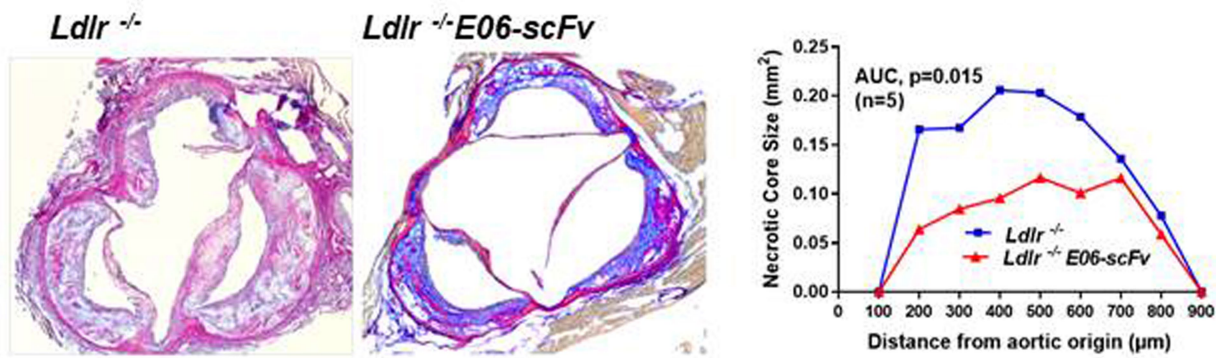
red, annexin V-PE. **c**, Binding of E06-scFv plasma (1:20 dilution) to apoptotic thymocytes (7AAD⁺annexin V⁺) isolated by FACS analysis. **d**, Expression of E06-scFv in aortic lesion of a *Ldlr*^{-/-} E06-scFv but not a *Ldlr*^{-/-} mouse. Cross-sections at the aortic valve were stained with biotinylated anti-Myc monoclonal antibody to identify presence of E06-scFv in atherosclerotic lesion. Nuclei counterstained using haematoxylin QS (Original ×200). **a-c**, Representative of similar studies with five other plasma samples from each genotype. **d**, Representative of studies in three other aortic sections of each genotype.



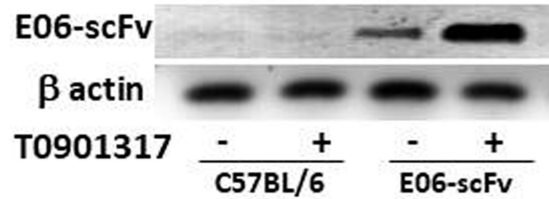
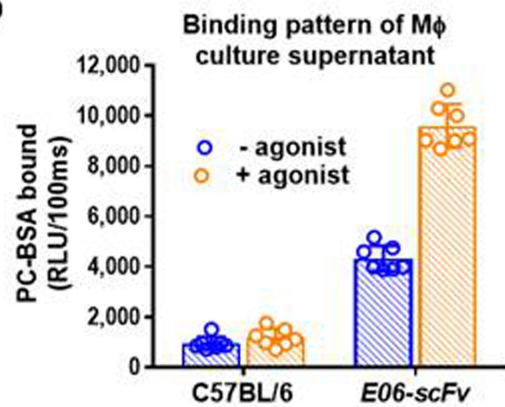
Extended Data Fig. 4 | Lipoprotein profiles of $Ldlr^{-/-}$ and $Ldlr^{-/-}$ E06-scFv mice are similar in various studies. a, b, Distributions of plasma cholesterol (a) and triglycerides (b) by fast performance liquid chromatography in pools of equal aliquots of plasma from mice fed a HCD for 4 months ($Ldlr^{-/-}$ $n = 10$, $Ldlr^{-/-}$ E06-scFv $n = 11$). c, Plasma

cholesterol distribution in mice fed a HCD for 7 months ($Ldlr^{-/-}$ $n = 9$, $Ldlr^{-/-}$ E06-scFv $n = 7$). d, Plasma cholesterol and triglyceride distribution in BMT experiment: lipoprotein profiles in $Ldlr^{-/-}$ mice that received bone marrow from wild-type (control, $n = 9$) or E06-scFv ($n = 13$) mice and tjtat were then fed a Western diet for 16 weeks.

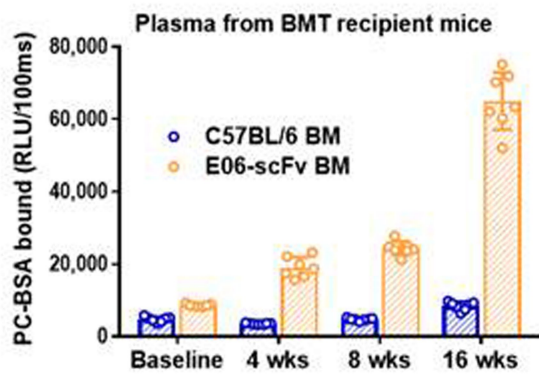
a



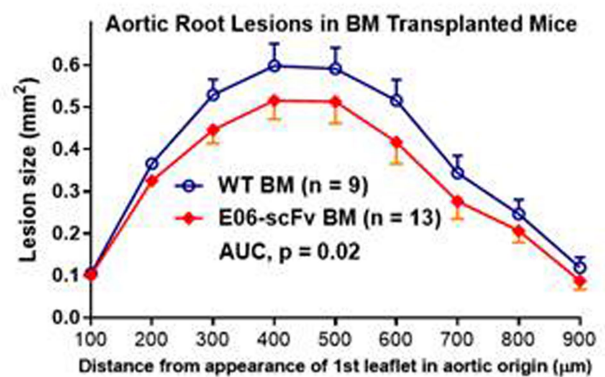
b



c



d

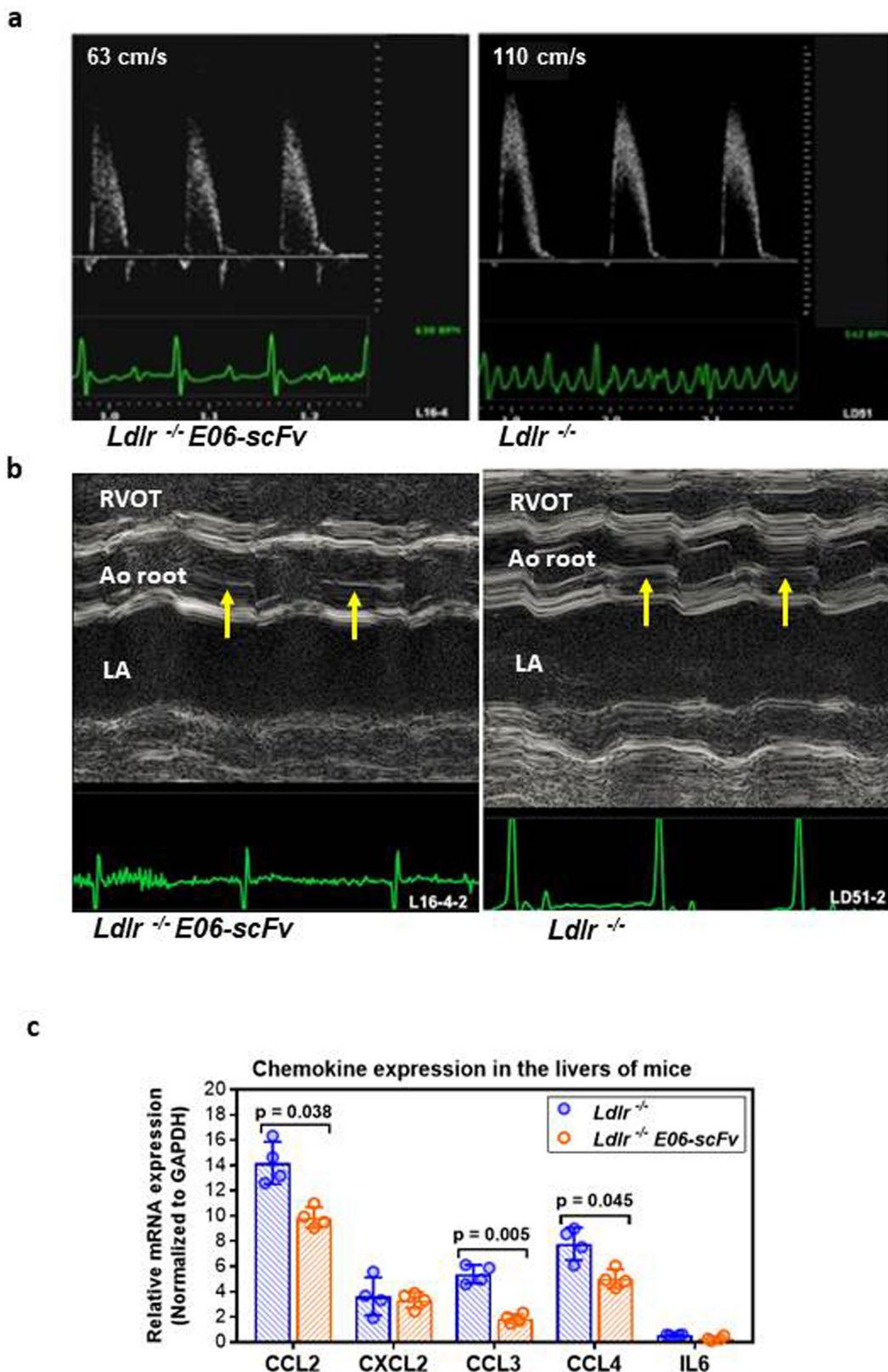


Extended Data Fig. 5 | See next page for caption.

Extended Data Fig. 5 | E06-scFv reduces necrotic core formation and macrophage secretion of E006-scFv confers atheroprotection.

a, E06-scFv reduces extent of necrosis within aortic root lesions after a HCD for seven months as shown in Fig. 2c. Lesions of equal size were matched at each of the indicated sites in aortic root sections from 7 *Ldlr*^{-/-} and 9 *Ldlr*^{-/-}-E06-scFv mice and the extent of necrosis was measured as described in the Methods. Necrosis was reduced by 43.9% in *Ldlr*^{-/-}-E06-scFv mice (AUC 113.4 versus 63.6, $P = 0.015$). **b**, Secretion of E06-scFv in cultured peritoneal macrophages in the absence or presence of LXR agonist T090137 from C57BL/6 (wild-type) and E06-scFv mice determined by phosphocholine-binding assay. Culture supernatants were concentrated tenfold for ELISA (left). E06-scFv expression, driven by the *ApoE* promoter was stimulated by T0901317 as indicated by western blots of cell lysates with anti-Myc monoclonal antibody (right). Representative

of four separate experiments. **c**, Plasma E06-scFv titres following transplantation (baseline) in *Ldlr*^{-/-} mice transplanted with wild-type ($n = 7$) or E06-scFv ($n = 7$) bone marrow. E06-scFv titres (plasma from $n = 7$ wild-type and 7 E06-scFv mice) increased in mice transplanted with E06-scFv bone marrow over 16 weeks of Western diet. **d**, Aortic root atherosclerosis in *Ldlr*^{-/-} mice transplanted with wild-type ($n = 9$) or E06-scFv ($n = 13$) bone marrow after 16 weeks of Western diet. As described in the Methods, aortic root lesion areas were quantified from serial sections (nine sections per mouse) cut through the aorta at the origins of the aortic valve leaflets and then stained with a modified van Geison solution. Lesions at aortic root were reduced by 37% in mice that received BMT from E06-scFv mice (AUC 69.6 versus 110.6, $P = 0.02$, two-sided *t*-test).



Extended Data Fig. 6 | Aortic valve echocardiography and hepatic gene expression. **a**, Representative pulse-wave Doppler-derived aortic jet velocities of a 12-month-old *Ldlr*^{-/-}E06-scFv (left) and *Ldlr*^{-/-} (right) mouse: ECG traces are shown in green. Representative of studies in $n = 9$ *Ldlr*^{-/-} and 10 *Ldlr*^{-/-}E06-scFv mice. **b**, Representative M-mode echocardiography images containing the aortic valves in the short axis through the right ventricular outflow tract (RVOT), aortic (Ao) root with

aortic valve, and left atrium (LA). The aortic valve (arrows), best observed in diastole, is thinner in *Ldlr*^{-/-}E06-scFv compared to *Ldlr*^{-/-} mice. ECG traces shown in green. Representative of studies in $n = 9$ *Ldlr*^{-/-} and 10 *Ldlr*^{-/-}E06-scFv mice. **c**, Decreased inflammatory gene expression in whole-liver extracts of *Ldlr*^{-/-} and *Ldlr*^{-/-}E06-scFv mice after 16 weeks of HCD. Relative mRNA levels were determined by qPCR and normalized to *Gapdh* and expressed as mean \pm s.e.m. $n = 4$ mice per group.

Extended Data Table 1 | Weights and lipid levels in mice in atherogenic studies

a

Time Course Groups	-2 weeks (Baseline)		4 weeks		8 weeks		4 months		7 months		12 months	
	<i>Ldlr</i> ^{-/-}	E06-scFv	<i>Ldlr</i> ^{-/-}	E06-scFv	<i>Ldlr</i> ^{-/-}	E06-scFv	<i>Ldlr</i> ^{-/-}	E06-scFv	<i>Ldlr</i> ^{-/-}	E06-scFv	<i>Ldlr</i> ^{-/-}	E06-scFv
Weight (g) ± SEM	25.1 ±0.5	22 ±1.1	27.5 ±0.5	24 ±1.1	28.2 ±0.5	24.9 ±1.1	30.7 ±0.6	26.7 ±1.3	35.2 ±4.2	34.8 ±3.6	38.7 ±7.6	37.3 ±4.1
Total Chol (mg/dL)	269 ±9.5	246 ±9.9	944 ±63	957 ±52	852 ±55	925 ±46	624 ±38	881 ±125	790 ±240	937 ±135	1108 ±467	1119 ±409
Triglyceride (mg/dL)	88 ±9.2	139 ±9.7	135 ±12	141 ±17	111 ±7.5	123 ±12	128 ±7.7	151 ±14	161 ±54	199 ±78	162 ±51	249 ±92

b

Time Course Groups	-2 weeks (Baseline)		4 weeks		8 weeks (Midpoint)		16 weeks (Endpoint)	
	C57BL	E06-scFv	C57BL	E06-scFv	C57BL	E06-scFv	C57BL	E06-scFv
Weight (g) ± SEM	22.3 ±1.6	23.4 ±2.4	24.5 ±1.7	25 ±2.4	26.2 ±0.7	26.1 ±2.9	26.8 ±1.7	27.4 ±2.4
Total Chol (mg/dL)	248 ±23	240 ±25	1231 ±64	1328 ±95	1444 ±140	1240 ±143	1579 ±168	1215 ±216
Triglyceride (mg/dL)	92 ±16	112 ±30	176 ±50	202 ±53	143 ±25	178 ±44	578 ±83	433 ±62

a. Indicated parameters for mice on HCD diets for 4-, 7- or 12-month studies. Results represent the mean ± s.e.m. For mice on the 4-month diet protocol, plasma cholesterol and triglyceride were measured at baseline, 4 weeks, 8 weeks and at 4 months. For mice in the 7- and 12-month protocols, measurements were made at the end point. There were no significant differences between mice at any given time point. For the 4-, 7- and 12-month protocols, $n = 10, 9, 8$ *Ldlr*^{-/-} and $n = 11, 7, 10$ *Ldlr*^{-/-}-E06-scFv mice, respectively.

b. Variables at indicated times in *Ldlr*^{-/-} recipient mice on the Western diet following BMT from C57BL/6 or E06-scFv mice on C57BL/6 background. Results represent the mean ± s.e.m. There are no significant differences between mice at any given time point. Number of mice for C57BL/6 donors, $n = 9$; for E06-scFv donors, $n = 13$.

Extended Data Table 2 | Gene Ontology analysis of differentially expressed genes in macrophages of *Ldlr*^{-/-} and *Ldlr*^{-/-}E06-scFv mice

Go Analysis: Genes Expression > 1.5 fold higher in E06-scFv Transgenic Mice			
Term	Count	%	P-value
GO:0006955 ~ immune response	45	16.4234	9.37E-26
GO:0009615 ~ response to virus	12	4.3796	3.69E-09
GO:0002684 ~ positive regulation of immune system process	17	6.2044	1.12E-08
GO:0045087 ~ innate immune response	13	4.7445	1.39E-08
GO:0006952 ~ defense response	24	8.7591	1.89E-08
GO:0050778 ~ positive regulation of immune response	14	5.1095	2.40E-08
GO:0002460 ~ adaptive immune response based on somatic recombination of immune receptors built from immunoglobulin superfamily domains	11	4.0146	1.31E-07
GO:0002250 ~ adaptive immune response	11	4.0146	1.31E-07

Gene Ontology (GO) analysis of genes that were increased >1.5-fold in TGEM of *Ldlr*^{-/-}E06-scFv mice compared to *Ldlr*^{-/-} mice. Experimental details and major gene changes are shown in Fig. 3. Data of TGEM from *n* = 4 mice per group.

Extended Data Table 3 | Cell counts of viable aortic cells determined using FACS analysis

Group	Total Viable cells*	Monocytes (% of Total)	Lymphocytes (% of Total)	B cells (% of Lymph)	T cells (% of Lymph)
HCD <i>E06-scFv</i>	3398 ±2615	43 ± 7.1	57 ± 7.1	4.1 ±2.0	54 ± 11
Chow- <i>Ldlr</i> ^{-/-}	864 ± 1085	43 ± 15	57 ± 15	7.5 ±5.1	29 ± 15
HCD- <i>Ldlr</i> ^{-/-}	7829** ±10,247	18 ± 4.6	82 ± 4.6	12 ± 20	62 ± 15

Cell counts of viable aortic cells isolated from aortas of chow-fed and HCD-fed *Ldlr*^{-/-} mice and HCD-fed *Ldlr*^{-/-}*E06-scFv* mice. Values are mean ± s.d. of total viable cells evaluated by flow cytometry per aorta as described in the Methods. Number of aorta for each group: *n* = 5 HCD-fed *Ldlr*^{-/-}*E06-scFv* mice; *n* = 6 chow-fed *Ldlr*^{-/-} mice and *n* = 6 HCD-fed *Ldlr*^{-/-} mice.

*Note that one aorta from one HCD-fed *Ldlr*^{-/-} mouse had extensive atherosclerosis and had 27,846 viable cells counted. The next highest value in this group was 9,342. By comparison, the highest in the Chow-fed *Ldlr*^{-/-} group was 2,909 and in the HCD-*Ldlr*^{-/-}*E06-scFv* group was 5,692. Aortic cells were evaluated by flow cytometry as described in the Methods. Data for phenotypes of monocyte/macrophages are shown in Fig. 3.

Extended Data Table 4 | Echocardiographic parameters of mice after 12 months of HCD

Parameters	<i>Ldlr</i> ^{-/-} (n=13)	<i>Ldlr</i> ^{-/-} E06-scFv (n=10)	P value
HR (bpm)	528±55	562±51	0.18
IVSd (mm)	0.75±0.08	0.73±0.05	0.55
LVIDd(mm)	3.68±0.45	3.76±0.39	0.67
LVIDs(mm)	2.51±0.42	2.60±0.43	0.63
LVPWd(mm)	0.73±0.08	0.71±0.07	0.54
%FS	31.8±7.3	31.0±7.9	0.78
LVM/BW	25.2±5.0	25.6±4.1	0.84
Aortic Valve			
-Peak Velocity (cm/s)	103.22±28.23	79.25±29.50	0.020
-Peak Gradient (mmHg)	4.56±2.43	2.83±1.91	0.025

Values are mean ± s.d. and *P* values refer to comparisons between *Ldlr*^{-/-} and *Ldlr*^{-/-}E06-scFv mice using a two-sided *t*-test. FS, fractional shortening; HR, heart rate; IVSD, interventricular septum during diastole; LVIDd, left ventricular internal diameter during diastole; LVIDs, left ventricular internal diameter during systole; LVPWd, left ventricular posterior wall thickness during diastole; LVM/BW, ratio of left ventricle mass to body weight. This table includes studies in 2 *Ldlr*^{-/-} mice that were not included in Fig. 4a.

Reporting Summary

Nature Research wishes to improve the reproducibility of the work that we publish. This form provides structure for consistency and transparency in reporting. For further information on Nature Research policies, see [Authors & Referees](#) and the [Editorial Policy Checklist](#).

Statistical parameters

When statistical analyses are reported, confirm that the following items are present in the relevant location (e.g. figure legend, table legend, main text, or Methods section).

n/a Confirmed

- The exact sample size (n) for each experimental group/condition, given as a discrete number and unit of measurement
- An indication of whether measurements were taken from distinct samples or whether the same sample was measured repeatedly
- The statistical test(s) used AND whether they are one- or two-sided
Only common tests should be described solely by name; describe more complex techniques in the Methods section.
- A description of all covariates tested
- A description of any assumptions or corrections, such as tests of normality and adjustment for multiple comparisons
- A full description of the statistics including central tendency (e.g. means) or other basic estimates (e.g. regression coefficient) AND variation (e.g. standard deviation) or associated estimates of uncertainty (e.g. confidence intervals)
- For null hypothesis testing, the test statistic (e.g. F , t , r) with confidence intervals, effect sizes, degrees of freedom and P value noted
Give P values as exact values whenever suitable.
- For Bayesian analysis, information on the choice of priors and Markov chain Monte Carlo settings
- For hierarchical and complex designs, identification of the appropriate level for tests and full reporting of outcomes
- Estimates of effect sizes (e.g. Cohen's d , Pearson's r), indicating how they were calculated
- Clearly defined error bars
State explicitly what error bars represent (e.g. SD, SE, CI)

Our web collection on [statistics for biologists](#) may be useful.

Software and code

Policy information about [availability of computer code](#)

Data collection

Graph Pad Prism 7.04(trial version), Image Pro Plus 6.3, Flo-Jo 9.7, Rotor-Gene Q Software 1.7 (Quiagen), Cuffdiff2 TreeView-version 6, David6.7, DEseq2,--all added to Methods

Data analysis

no custom software used. Description of data handling of RNAseq is provided in detail in the Methods.

For manuscripts utilizing custom algorithms or software that are central to the research but not yet described in published literature, software must be made available to editors/reviewers upon request. We strongly encourage code deposition in a community repository (e.g. GitHub). See the Nature Research [guidelines for submitting code & software](#) for further information.

Data

Policy information about [availability of data](#)

All manuscripts must include a [data availability statement](#). This statement should provide the following information, where applicable:

- Accession codes, unique identifiers, or web links for publicly available datasets
- A list of figures that have associated raw data
- A description of any restrictions on data availability

Data Availability: The datasets generated during and/or analysed during the current study are available from the corresponding author on reasonable request. The raw sequence data presented in this article have been submitted to the National Center for Biotechnology Information Sequence Read Archive (<https://www.ncbi.nlm.nih.gov/sra/>, BioProject) under accession number PRJNA438959.

Field-specific reporting

Please select the best fit for your research. If you are not sure, read the appropriate sections before making your selection.

Life sciences Behavioural & social sciences

For a reference copy of the document with all sections, see nature.com/authors/policies/ReportingSummary-flat.pdf

Life sciences

Study design

All studies must disclose on these points even when the disclosure is negative.

Sample size	For various atherosclerosis studies, sample sizes were selected based on many years of experience; roughly 10-13 mice per experimental group were used: we conducted 5 separate studies over 3 years and so results involve > 100 mice in total and we feel results are robust. For other experiments, biological replicates were of size to provide confidence in measurements. Numbers of mice used in each experiment are recorded in figures and/or legends
Data exclusions	For the experiments, the data are reported in full. In the roughly 100+ mice studied in the various atherosclerosis studies, we found one mouse that had a bicuspid aortic valve and there was enhanced lesion around this but as this was a rare and single event, we did exclude this one mouse. Not mentioned in Methods or results as such a rare event. All other data are defined in Legends of each experiment.
Replication	The number of mice studied, or number of biological observations studied for each experiment are provided in figures or legends in every case.
Randomization	For atherosclerosis studies, Ldlr or Ldlr/E06-scFv-Tg mice were matched for age/sex (male) and baseline cholesterol for each of the studies.
Blinding	For the main findings: the analysis of extent of atherosclerosis or the changes in flow dynamics across the aortic valve--were done in blinded fashion by those who performed these analyses.

Materials & experimental systems

Policy information about [availability of materials](#)

n/a	Involvement in the study
<input type="checkbox"/>	<input checked="" type="checkbox"/> Unique materials
<input type="checkbox"/>	<input checked="" type="checkbox"/> Antibodies
<input type="checkbox"/>	<input checked="" type="checkbox"/> Eukaryotic cell lines
<input type="checkbox"/>	<input checked="" type="checkbox"/> Research animals
<input type="checkbox"/>	<input checked="" type="checkbox"/> Human research participants

Unique materials

Obtaining unique materials There are no unique reagents available only to us. The E06 antibody is commercially available now (see below). We made the E06-scFv transgenic mice --which are unique--and will make them available to interested investigators in the future.

Antibodies

Antibodies used All antibodies used are described in Materials and Methods. The IgM E06 is now available from Avanti Polar Lipids. The manuscript describes in detail the generation of the E06-scFv and its validation. Arrangements are being made to have Avanti generate and make available the E06-scFv as well.

Validation Aside from the E06 antibody, which has been extensively characterized in the literature as described in Supplemental Information, the antibodies used in the FACS analysis are all listed in the Methods or in Supplemental Information. Antibody

AB1-2 to the E06/T15 idiotype was originally provided to us several decades ago by J. Kearney U Alabama, but hybridoma is available from ATCC.

Eukaryotic cell lines

Policy information about [cell lines](#)

Cell line source(s)	Only standard lines J774, HEK293 and Jurkat were used as described in Methods. The J774 cell line has been been in the UCSD Atherosclerosis cell culture core since I arrived at UCSD more than 39 years ago. No one knows the original source. HEK293 and JURKAT were originally from ATCC.
Authentication	These cell lines have not been authenticated.
Mycoplasma contamination	We routinely survey our dedicated cell culture laboratory (which is used only by our group) for mycoplasma but I am unaware if we specifically tested for mycoplasma in cells lines immediately prior to use in these experiments. .
Commonly misidentified lines (See ICLAC register)	None of the 3 cell lines used are listed in the register

Research animals

Policy information about [studies involving animals](#); [ARRIVE guidelines](#) recommended for reporting animal research

Animals/animal-derived materials	All mice were on C57BL/6 background and included Ldlr ^{-/-} , Rag1 ^{-/-} and E06-scFv-Tg mice generated on C57BL/6 background bred into the LDLr ^{-/-} , or Rag1 ^{-/-} or Ldlr ^{-/-} x Rag1 ^{-/-} background. Mice were typically used from 3 month of age to as long as 15 month as described in the various protocols. Studies were not done in female mice.
----------------------------------	--

Human research participants

Policy information about [studies involving human research participants](#)

Population characteristics	Plasma was collected from healthy human volunteers for the specific purpose of isolation of LDL used in the generation of antigens to be tested in ELISA assays. UCSD IRB protocol is held by one of the authors for this purpose. There are no other human samples in these studies. A statement about informed consent and IRB approval is in Methods
----------------------------	---

Method-specific reporting

n/a	Involvement in the study
<input checked="" type="checkbox"/>	<input type="checkbox"/> ChIP-seq
<input type="checkbox"/>	<input checked="" type="checkbox"/> Flow cytometry
<input checked="" type="checkbox"/>	<input type="checkbox"/> Magnetic resonance imaging

Flow Cytometry

Plots

Confirm that:

- The axis labels state the marker and fluorochrome used (e.g. CD4-FITC).
- The axis scales are clearly visible. Include numbers along axes only for bottom left plot of group (a 'group' is an analysis of identical markers).
- All plots are contour plots with outliers or pseudocolor plots.
- A numerical value for number of cells or percentage (with statistics) is provided.

Methodology

Sample preparation	None of the original FACS data are presented in the revised paper due to space limitations. These studies were conducted by Dr. Klaus Ley at the LIAI who is a world authority in these studies. Details of studies are supplied in detail in Methods.
Instrument	LSRII as well as FACSCanto and FACSAria (BD Bioscience, San Diego, CA)Details for relevant experiments are provided in Methods
Software	Flow Jo 9.7 (Tree Star Inc., Ashland, OR).
Cell population abundance	Numbers are provided for the cell sorting of aortic cells--which can be found in Extended Data Table 3.
Gating strategy	Examples of gating strategy were presented in the Extended Data of original version but have been deleted due to formatting of paper to Letter format. This had been shown in Added Data section for novel analysis of lymph nodes/spleen and blood: A reference is provided in Methods for the cell sorting strategy of aortic cells, performed in the LIAI lab under direction of Klaus Ley, who is considered a world leader. Gating strategy to define the macrophage cell types shown in Fig 3f are defined in both Results and Legend to define explicit markers used to define populations reported.

- Tick this box to confirm that a figure exemplifying the gating strategy is provided in the Supplementary Information.